NASA CONTRACTOR REPORT

NASA CR-2747

TRANSONIC PERFORMANCE OF A MACH 2.65 AUXILIARY FLOW AXISYMMETRIC INLET

Don M. Santman

Prepared by
ELLCO ENGINEERING, INC.
Compton, Calif.
for Ames Research Center

NATIONAL AERONAUTICS AND SPACE ADMINISTRATION • WASHINGTON, D. C. • OCTOBER 1976

1. Report No.	2. Government Accession No.	3. Recipient's Catalog No.
NASA CR-2747		

4. Title and Subtitle	5. Report Date
Transonic Performance of a Mach 2.65 Auxiliary Flow Axisymmetric Inlet	OCTOBER 1976
	6. Performing Organization Code
7. Author(s)	8. Performing Organization Report No.
Don M. Santman	
	10. Work Unit No.
9. Performing Organization Name and Address	11. Contract or Grant No.
Ellco Engineering, Inc. Compton, California	NAS 2-8679
	13. Type of Report and Period Covered
12. Sponsoring Agency Name and Address	Contractor report
National Aeronautics and Space Administration Washington, D.C. 20546	14. Sponsoring Agency Code

15. Supplementary Notes Program Managers: Norman E. Sorensen and Eldon A. Latham
Aerodynamics Branch
NASA, Ames Research Center
Moffett Field, California 94035

16. Abstract

Transonic experimental performance for a large scale Mach 2.65 axisymmetric inlet model with auxiliary airflow systems are presented. The inlet model incorporated both centerbody and cowl auxiliary airflow systems. When the centerbody system was fully open the performance at the simulated compressor face was such that, at 0.10 total-pressure distortion the total capture mass-flow ratio increased 0.055 and 0.051 and the total-pressure recovery increased 0.015 and 0.012 at Mach 0.9 and 1.3, respectively. Flow separation on the centerbody resulted in supercritical centerbody auxiliary throat flow prior to attainment of choked main duct throat flow. Cowl auxiliary airflow had a detrimental effect on compressor-face performance. To overcome the detrimental effect, alternate cowl auxiliary airflow systems are described for efficient merging of auxiliary and main duct airflows and for providing similar auxiliary and main duct throat flow choking characteristics.

17. Key Words (Suggested by Author(s))	18. Distribution Statement
Axisymmetric, Inlet, Transonic, Supersonic, Auxiliary Flow, Propulsion System	Unclassified-Unlimited STAR Category 07

19. Security Classif. (of this report)	20. Security Classif. (of this page)	21. No. of Pages	22. Price*
Unclassified	Unclassified	61	$4.25

For sale by the National Technical Information Service, Springfield, Virginia 22161

TRANSONIC PERFORMANCE OF A MACH 2.65 AUXILIARY FLOW AXISYMMETRIC INLET

By Don M. Santman
Ellco Engineering Incorporated

SUMMARY

Transonic wind tunnel test results for a large scale auxiliary airflow axisymmetric inlet model designed for Mach 2.65 are presented. The inlet is a mixed-compression translating centerbody type with a cowl lip diameter of 50.8 cm. The inlet incorporated both centerbody and cowl auxiliary airflow systems to augment the main duct transonic airflow capacity. The on-design subsonic diffuser is short relative to current designs resulting in an inlet only 1.63 cowl lip diameters long measured from the cowl lip to the compressor face.

Major objectives of the test were to obtain compressor-face performance data with and without auxiliary airflow, to determine maximum transonic capture airflow for acceptable engine operation, and to determine auxiliary and main duct airflow matching characteristics. Also, subsonic diffuser performance with the centerbody located in the Mach 2.65 design position was to be evaluated. The tests were conducted over the Mach number range from 0.6 to 1.3 and angles of attack up to eight degrees at subsonic Mach numbers and four degrees at supersonic Mach numbers.

The fully open centerbody auxiliary system provided compressor-face performance such that, at 0.10 total-pressure distortion, the total capture mass-flow ratio increased 0.055 and 0.051 and the total-pressure recovery increased 0.015 and 0.012 at Mach 0.9 and 1.3, respectively. Test results indicated that operation of the centerbody auxiliary system resulted in main duct flow separation on the centerbody. This separation reduced the effective main duct flow area at the auxiliary duct exit station and permitted choking of the auxiliary duct throat flow prior to choking of the main duct throat flow.

Cowl auxiliary airflow had a detrimental effect on compressor-face total-pressure recovery and distortion. Replacement of the cowl auxiliary duct porous bypass screen, which separates the auxiliary duct plenum and main diffuser duct, with a flap arrangement is recommended to provide efficient merging of auxiliary and main duct airflows. Simultaneous choking of auxiliary and main duct throat flows was not achieved at supersonic Mach numbers because of reduced auxiliary airflow recoveries. A flap arrangement which provides auxiliary duct exit area adjustment is recommended to provide similar choking characteristics. Achievement of acceptable cowl auxiliary duct performance at Mach 1.3 is questionable because of strong shock boundary-layer interaction effects upstream of the auxiliary duct entrance.

A high subsonic diffuser total-pressure recovery of 0.965 and a compressor-face total-pressure distortion of 0.10 was achieved with the centerbody located in the on-design position and with a throat Mach number of 0.8.

INTRODUCTION

Mixed-compression axisymmetric inlets are receiving increased study for use on advanced supersonic transport aircraft (refs. 1, 2 and 3). Potential installed performance benefits such as reduced weight and drag with high internal performance prompts selection of axisymmetric rather than two-dimensional inlets. Realization of these benefits, however, is hampered because of inherently low transonic airflow capability of this type of inlet with only a translating centerbody for off-design operation.

One way of increasing the transonic airflow capability to satisfy the airflow demands of most engines is through use of collapsing rather than translating centerbody systems. The practicality of these systems, however, is doubtful considering leakage and boundary-layer bleed compartmentalization problems associated with a multi-segmented centerbody. Attempts to increase the transonic airflow of translating centerbody systems by reducing the centerbody maximum diameter results in a centerbody design which requires a "traveling" bleed system. That is, the reduced centerbody diameter forces the geometric throat to remain fixed on the cowl. Thus, the centerbody throat bleed must shift or "travel" with centerbody translation to remain opposite the fixed cowl throat bleed.

The intake developed by Boeing under the supersonic transport program employed a translating centerbody and a variable cowl (ref. 4). The variable cowl provided increased transonic airflow capability by increasing the inlet throat area. Although the variable cowl system was mechanically practical, it was relatively complex and accounted for a large fraction of the inlet weight. The inlet also employed a centerbody traveling bleed system. A simplified inlet was subsequently developed by NASA Ames (ref. 5) which employed a fixed cowl. Transonic airflow considerations required, however, that the inlet be oversized at the cruise Mach number which resulted in increased weight and drag.

Centerbody and cowl auxiliary airflow systems which augment the airflow capability of translating centerbody inlets have been proposed by NASA Ames (ref. 6). Centerbody auxiliary airflow is achieved by aft translation of the forward portion of the centerbody to create an annular opening which permits auxiliary airflow to pass through the centerbody and merge with the main duct airflow. The proposed cowl auxiliary system employs external cowl scoops which open to allow auxiliary airflow to pass through the cowl. Application of either auxiliary airflow system permits the maximum centerbody diameter to be increased sufficiently to eliminate the need for a centerbody traveling bleed system. That is, as the centerbody translates for off-design operation, the geometric throat remains fixed on the centerbody rather than on the cowl. Elimination of the traveling bleed system also permits a reduction in subsonic diffuser length by allowing the centerbody support struts to penetrate the aft portion of the centerbody.

This report presents an experimental evaluation of centerbody and cowl auxiliary airflow systems installed in a Mach 2.65 mixed-compression inlet. The test inlet was approximately a 1/3-scale model of the auxiliary inlet concept developed by the NASA Ames Research Center. Model design, fabrication, and testing was conducted by Ellco Engineering, Inc. The Los Angeles Aircraft Division of Rockwell International provided testing assistance. The test was conducted in the NASA Ames 11-by 11-ft Unitary Plan Wind Tunnel Facility over the Mach Number range from 0.6 to 1.3 and for angles of attack up to 8 degrees at subsonic Mach numbers and 4 degrees at supersonic Mach numbers.

Major objectives of the test were to obtain the effect of auxiliary airflow on compressor-face performance, to determine maximum transonic capture airflow for acceptable engine operation, and to determine auxiliary and main duct airflow matching characteristics. Also, the performance of the short subsonic diffuser with the centerbody located in the Mach 2.65 position was to be determined.

SYMBOLS

A_C	cowl auxiliary duct throat area
A_{CB}	centerbody auxiliary duct throat area
A_L	cowl lip area
A_X	flow area at inlet station X
h	duct height
M_L	freestream Mach number
M_{TH}	inlet main duct throat Mach number
P	static pressure
P_{PL}	cowl auxiliary duct plenum static pressure
P_T	total pressure
P_{TAV}	area weighted total pressure at compressor face
P_{TC}	area weighted total pressure at cowl auxiliary duct entrance
P_{TCB}	area weighted total pressure at centerbody auxiliary duct exit
P_{TI}	inlet main duct flow area weighted total pressure
P_{TMAX}	maximum total pressure at compressor face
P_{TMIN}	minimum total pressure at compressor face
P_{TO}	freestream total pressure
P_{TR}	average compressor face ring recovery
R	radius
R_L	cowl lip radius

t	thickness
W	weight flow
W_C	cowl auxiliary airflow
W_{CB}	centerbody auxiliary airflow
W_I	inlet main duct airflow
W_L	theoretical freestream flow through area equal to cowl lip area
W_T	inlet total capture airflow
X	inlet station (X = O at centerbody tip station with centerbody in forward transonic position)
Z	cowl auxiliary duct width
ΔR	distance from surface
ΔX_{CB}	centerbody translation from full forward position (X = 0)
ΔX_{FC}	forecone translation from full forward position (X = 0)
α	angle of attack

TEST APPARATUS

Model Description

The test inlet was a Mach 2.65 axisymmetric inlet model which incorporated centerbody and cowl auxiliary airflow systems. The inlet was a mixed-compression translating centerbody type with a cowl lip diameter of 50.8 cm (approximately 1/3 scale). A schematic representation of the inlet is presented in figure 1. Model photographs are presented in figures 2 and 3.

Centerbody translation was achieved manually. The aft section of the centerbody was slotted to accommodate the centerbody support struts with the centerbody in the Mach 2.65 (on-design) position (illustrated in upper portion of figure 1). Removable centerbody fairings were located between the support struts. These fairings reduce the size of the aft facing step at the exit of the centerbody auxiliary airflow system with the centerbody in the on-design position. Triangular vortex generators were located on the cowl and centerbody. The vortex generators were arranged in pairs as illustrated in figure 4. Cowl and centerbody on-design contours are presented in table I. Table II presents support strut and centerbody fairing contours.

The centerbody was designed so that the forecone could be remotely actuated to allow auxiliary airflow to pass through the centerbody to the simulated compressor face (see lower portion of figure 1). The centerbody contained an annular internal passageway which transitioned into twelve flow ducts by use of the webs illustrated in sections B-B and C-C of figure 1. The webs simulate the external dimensions of the hollow webs which would be required to pass the bleed flow of an actual inlet with a boundary layer bleed system (a bleed system is required to control boundary-layer separation during started inlet operation at supersonic speeds).

Referring to the area distributions presented in figure 5, the full aft forecone position ($\Delta X_{FC}/R_L$ = 1.38) resulted in an auxiliary duct throat to capture area ratio (A_{CB}/A_L) of 0.107. Combining this throat area with that of the main duct with the centerbody located in the transonic position results in a total throat to capture area ratio of 0.632. Although this combined throat area would permit a theoretical maximum capture mass-flow ratio of 0.632 at Mach 1.0 which approximately equals the airflow capability of the U.S. SST prototype inlet system (ref. 6), a second geometric throat located in the diffuser duct at station X/R_L = 6.64 (mid-plane of centerbody support struts) limits the maximum total capture mass-flow ratio to a value of 0.568. This latter throat was formed as a result of the short subsonic diffuser design combined with relatively thick centerbody support struts which simulate the thickness required to pass the centerbody bleed flow of an actual inlet.

The model contained four manually positioned cowl doors which form scoops allowing cowl auxiliary airflow to pass through the porous bypass screens to the simulated compressor face. Two door positions which result in auxiliary duct entrance areas of 10 and 20 percent of inlet capture area were available. The cowl door inner surface was contoured to achieve a linear duct Mach number distribution assuming Mach 1.0 at the entrance (station X/R_L = 5.635) and Mach 0.3 at the duct exit into the plenum (station X/R_L = 6.235). The auxiliary duct sidewalls were parallel. The duct width was sufficient to admit auxiliary flow over the entire circumference between the support struts.

The bypass screen consists of 0.098 cm diameter holes spaced to provide a porosity of 40 percent. Blank-off plates for reducing the screen open area by 50 percent were also available. The plates were installed on the plenum side of the screen between stations X/R_L = 6.543 and X/R_L = 6.848 just upstream of the compressor face.

The inlet was mounted to a NASA-Ames supplied sting-body assembly which contained a flow control plug. The flow control plug and the inlet forecone were remotely positioned using electrohydraulic servo control valves.

Instrumentation

Pressure data acquisition was accomplished through use of twelve 24-port scanivalves located within the inlet diverter. The inlet static and total-pressure instrumentation consisted of the following.

- Fifty-two internal cowl and centerbody surface static taps and fourteen external cowl static taps.
- Four cowl auxiliary duct plenum statics.

- Two six-probe total-pressure rakes located in the main duct at the throat station ($X/R_L = 4.31$). These rakes were used for calibration of the main duct airflow and were installed only during calibration tests.

- Two six-probe total-pressure rakes located within two of the centerbody auxiliary flow ducts at station $X/R_L = 3.7$. These rakes were used for calculating centerbody auxiliary airflow.

- Two six-probe total-pressure rakes located at the cowl auxiliary duct entrance ($X/R_L = 5.635$). These rakes were used for calculating cowl auxiliary airflow.

- Two twelve-probe total-pressure rakes located at station $X/R_L = 5.175$ coincident with the centerbody auxiliary duct exit. Six probes of each rake were utilized for survey of the auxiliary duct exit flow while the remaining six probes were used for survey of the main duct flow. These rakes were installed only for the survey tests.

Compressor-face instrumentation, located in the sting-body assembly, consisted of 56 total-pressure probes. The rake consisted of eight seven-probe arms.

ON-DESIGN DIFFUSER PERFORMANCE

Test results illustrating vortex generator and centerbody fairing effects on subsonic diffuser performance are presented in this section. The tests were conducted with the centerbody in the Mach 2.65 design position which results in a very short subsonic diffuser and high adverse pressure gradients. Although the tests were conducted at a freestream Mach number of 0.9 rather than Mach 2.65, the results provide an indication of the subsonic diffuser performance to be expected at Mach 2.65. Specifically, test results obtained with a throat Mach number of approximately 0.8 (Mach number downstream of a Mach 1.25 terminal shock) may be representative of the performance obtained with a throat Mach number of 1.25 (Mach 2.65 operation) provided the terminal shock is near the throat and sufficient boundary-layer bleed is used to prevent boundary-layer separation downstream of the terminal shock boundary-layer interaction.

Vortex Generator Effects

The cowl vortex generators had a detrimental effect on compressor-face performance. Compressor-face recovery and distortion data illustrating this effect are presented in figure 6 as a function of throat Mach number. For a throat Mach number of 0.8 the recovery is reduced 0.04 and the distortion is increased 0.04 by installation of the cowl vortex generators. Compressor-face rake total-pressure profiles presented in figure 7 for a throat Mach number of 0.75 show that the reduced performance is due to formation of a low recovery region near the cowl. Also, localized cowl flow separation occurs in the lower right quadrant (rake 4, looking aft) upon installation of the cowl vortex generators.

Cowl surface static pressure distributions presented in figure 8 for a throat Mach number of 0.75 indicate that cowl flow separation is occurring at approximately $X/R_L = 6.1$ which is coincident with the location of the cowl vortex generators. The pressure distributions indicate that

the separation point is not influenced by either installation or removal of the cowl vortex generators. Installation of the cowl vortex generators apparently increases the separation length which results in the low recovery flow region near the cowl at the compressor-face station, as indicated in figure 7. If the separation mechanism is the adverse pressure gradient associated with area divergence, relocation of the cowl vortex generators may improve the performance. However, if flow recirculation through the bypass screen is the separation mechanism, relocation of the generators would not significantly improve compressor-face performance.

Data illustrating the effect of installing both centerbody and cowl vortex generators are presented in figure 9. Due to model difficulties during the test run, test data were not obtained for subsonic throat Mach numbers greater than 0.75 with the vortex generators removed. Extrapolating the data to a throat Mach number of 0.8 indicates that the recovery would be reduced 0.045 and the distortion increased 0.04 by installation of both cowl and centerbody vortex generators. Although these increments are similar to those obtained by installation of only the cowl vortex generators (fig. 6) a direct comparison is not possible since the data shown in figure 9 were obtained with the centerbody fairing installed while the data presented in figure 6 were obtained with the centerbody fairing removed (centerbody fairing effects for a fixed vortex generator geometry are presented later).

Compressor-face rake profiles presented in figure 10 indicate a large recovery decrease near the cowl and a slight recovery increase near the centerbody upon installation of both cowl and centerbody vortex generators. These profile trends are similar to those obtained by installation of only the cowl vortex generators and indicate, therefore, that the centerbody vortex generators do not degrade the transonic performance. Vortex generator optimization studies at Mach 2.65 may indicate, however, that the generators are required to achieve an acceptable distortion level at the required stability margin.

Centerbody Fairing Effects

Compressor-face performance was improved by installation of the centerbody fairing. Installation of the fairing increased the recovery 0.005 and reduced the distortion approximately 0.015 for a throat Mach number of 0.80, as shown in figure 11. Installation of the fairing tends to divert the flow towards the centerbody. Compressor-face total-pressure profiles illustrated in figure 12, show that the flow redirection increases the recovery near the centerbody and decreases the recovery near the cowl except in the lower right quadrant where cowl flow separation is present. The data shown in figures 11 and 12 were obtained with the cowl and centerbody vortex generators installed. Thus, as previously indicated in figure 7, cowl flow separation in the lower right quadrant is expected.

Optimum Configuration

Optimum compressor-face performance was achieved with the vortex generators removed and the centerbody fairing installed. A high subsonic diffuser recovery of 0.965 and a distortion of 0.10 (considered acceptable for steady state engine operation) was achieved with a throat Mach number of approximately 0.8. As previously mentioned, this subsonic diffuser performance might also be achieved at Mach 2.65 provided that the terminal shock is near the throat (operation at critical point) and sufficient throat boundary-layer bleed is used to prevent boundary-layer separation downstream of the terminal shock boundary-layer interaction.

CENTERBODY AUXILIARY FLOW

Test results obtained with the centerbody located in the forward transonic position and with the forecone located in the forward, intermediate, and aft positions are presented. The latter two forecone positions result in centerbody auxiliary duct throat to capture area ratios (A_{CB}/A_L) of 0.053 and 0.107, respectively. The tests were conducted with only the centerbody vortex generators installed. The bypass screen blank-off plates were also installed.

Compressor-Face Performance

The centerbody auxiliary flow system appears to be a sound approach to increasing transonic airflow. That is, in general, an increased auxiliary duct throat area was accompanied by decreased total-pressure distortion and increased total-pressure recovery and maximum total capture flows. Figures 13 and 14 present compressor-face performance for freestream Mach numbers of 0.9 and 1.3, respectively. For a compressor-face distortion of 0.10, the full open auxiliary duct provides a 0.015 increase in compressor-face recovery and a maximum total capture mass-flow ratio increase ($\Delta W_T/W_L$) of 0.055 at Mach 0.9. At Mach 1.3, the auxiliary duct provides a 0.012 increase in recovery and a maximum total capture mass-flow ratio increase of 0.051.

As previously mentioned, the maximum total capture airflow with the full open auxiliary system is limited by choking at the diffuser duct throat formed in the strut region at $X/R_L = 6.64$. Assuming a choked diffuser throat flow, the theoretical maximum total capture mass-flow ratios are estimated to be 0.575 and 0.603 at Mach 0.9 and 1.3, respectively. The Mach 0.9 estimate assumes a diffuser throat total pressure equal to freestream total pressure. For the Mach 1.3 estimate, the diffuser throat total pressure was assumed equal to the total pressure downstream of a Mach 1.2 (centerbody forecone surface Mach number) terminal shock. As indicated in figures 13 and 14, the auxiliary system provides a theoretical maximum total capture mass-flow ratio increase ($\Delta W_T/W_L$), defined as the mass-flow ratio difference between a choked diffuser duct and a choked inlet main duct, of 0.043 and 0.045 at Mach 0.9 and 1.3, respectively.

At Mach 0.9, the characteristic drastic reduction in recovery at a fixed maximum capture mass-flow ratio was not obtained for the intermediate or full open auxiliary duct throat area settings (fig. 13). The reason for this was that the back pressure at the flow control plug was not sufficiently low to choke the flow at the diffuser throat (station $X/R_L = 6.64$). It was possible, however, to choke the inlet main duct flow with the auxiliary duct fully closed. At Mach 1.3 the back pressure was reduced sufficiently to achieve choked diffuser throat flow for all auxiliary duct throat area settings (fig. 14).

The maximum total capture mass-flow ratio obtained with the auxiliary duct full open exceeds the calculated maximum assuming choked diffuser throat flow (see figures 13 and 14). Airflow leakage through the bypass screens downstream of the diffuser throat is believed primarily responsible for this result eventhough blank-off plates were installed on the plenum side of the screens. The probable explanation is that the leakage flow path length was quite large since the blank-off plates were installed in four sections within each plenum chamber (four plates were required since three longitudinal webs were installed in the plenum chamber to provide structural support for the screens).

Duct Performance

The auxiliary duct exit area was sized to achieve simultaneous choking of the auxiliary and main duct throat flows with the auxiliary duct full open ($A_{CB}/A_L = 0.107$). Simultaneous choking is desirable since it results in a maximum recovery at the maximum capture airflow (both ducts choked). Specifically, an oversized auxiliary duct exit will result in supercritical auxiliary duct flow prior to choking of the main duct throat flow. Correspondingly, an undersized auxiliary duct exit will result in supercritical main duct flow prior to choking of the auxiliary duct throat flow. Thus, an improperly sized exit will cause premature choking in one of the ducts resulting in supercritical duct flow with excessive recovery losses prior to attainment of the maximum capture airflow.

The capture flow capability of the auxiliary and main ducts at Mach 0.9 and 1.3 are presented in figures 15 and 16, respectively. At the intermediate auxiliary duct opening ($A_{CB}/A_L = 0.053$), the auxiliary throat flow chokes prior to the main duct flow as evidenced by the near invariance of the auxiliary mass-flow ratio with total capture mass-flow ratio. This result is expected, as mentioned above, since the auxiliary duct exit to throat area ratio at the intermediate setting is larger than required for simultaneous choking of both duct throat flows.

Since the maximum total capture airflow was limited by choking at the diffuser duct throat formed in the strut region, it was not possible to choke both the auxiliary and main duct throat flows with the auxiliary duct full open ($A_{CB}/A_L = 0.107$). However, extrapolation of the mass-flow data to critical mass-flow values (indicated by horizontal dashed lines in figures 15 and 16) indicates that the auxiliary duct throat flow would also choke prior to choking of the main duct throat flow. This choking sequence is due to flow separation on the centerbody which reduces the effective main duct flow area at the auxiliary duct exit station.

Auxiliary and main duct total-pressure profiles at station $X/R_L = 5.175$ (auxiliary duct exit station) are presented in figure 17 which illustrates the centerbody flow separation obtained at Mach 0.9 with the full open auxiliary duct. Also presented are cowl and centerbody static pressure distributions. Centerbody flow separation is evident by a measured total pressure which is less than or equal to the interpolated static pressure indicated by dashed lines in figure 17. Flow separation occurs over the capture mass-flow ratio range tested and becomes more extensive at the lower capture airflows. The difference between the measured and predicted static pressure distributions (lower portion of figure 17) is not sufficient to locate the separation point.

For a fully closed auxiliary duct, main duct total-pressure profiles presented in figure 18 show that separation was evident at the low capture airflows but was not evident at the higher capture airflows where separation was obtained with the full open auxiliary duct. Similiar results were obtained at Mach 1.3 as shown in figure 19 which presents duct total-pressure profiles with and without auxiliary airflow. The results indicate that, at the high capture airflows, centerbody flow separation is induced by the presence of auxiliary airflow.

Separation occurs on the centerbody near the cowl lip station and the resulting low energy flow near the centerbody may be partly responsible for the main duct flow separation observed at the auxiliary duct exit station $X/R_L = 5.175$. Total-pressure profiles at the inlet main duct throat station ($X/R_L = 4.31$) which illustrates the low energy flow are presented in figure 20 for Mach numbers of 0.9 and 1.3. The low energy region is somewhat more extensive at Mach 1.3 because of terminal shock boundary-layer effects upstream of the cowl lip. The low energy region is also more

extensive at the low mass-flow ratios. Centerbody surface static pressure distributions upstream of the main duct throat are presented in figure 21 for a Mach number of 1.3. At the high capture mass-flow ratio the terminal shock is near the cowl lip and localized flow separation is present on the centerbody. This separation is evident because of the large difference between the measured and predicted internal duct pressure distributions near the cowl lip. At the lower mass-flow ratios, the separation in the cowl lip region becomes more extensive and reduces the effective lip flow area to result in approximately a constant static pressure between the lip and throat stations.

Auxiliary and main duct exit recovery characteristics at $X/R_L = 5.175$ and at the throat for the main duct are presented in figures 22 and 23 for Mach numbers of 0.9 and 1.3, respectively. For the intermediate auxiliary duct opening ($A_{CB}/A_L = 0.053$), supercritical auxiliary duct flow is present as evidenced by the large auxiliary airflow total-pressure recovery loss with increasing capture mass-flow ratio. With the auxiliary duct full open, the exit total-pressure recovery is relatively invarient with capture airflow indicating that the duct flow was not choked. The auxiliary duct total-pressure recovery data shown for the fully closed duct is merely the static pressure measured at the exit station.

The upper portions of figures 22 and 23 present inlet main duct total-pressure recovery at the throat ($X/R_L = 4.31$) and at the station corresponding with the auxiliary duct exit ($X/R_L = 5.175$). The throat total-pressure recovery is lower at the lower capture airflows because of separation upstream of the cowl lip (fig. 20). Also, terminal shock losses result in lower overall recoveries at Mach 1.3. The main duct flow total-pressure recovery loss between the throat and station $X/R_L = 5.175$ is due primarily to centerbody flow separation.

Compressor-Face Profiles

Compressor-face ring total-pressure recovery and distortion characteristics are presented in figures 24 and 25 for a Mach number of 0.9 and for various auxiliary duct throat areas. At the low capture mass-flow ratios the flow near the centerbody has the lowest total-pressure recovery. The total-pressure near the centerbody and the extent of high total-pressure core flow is increased as the auxiliary duct is opened because of increased auxiliary flow total-pressure recoveries. However, as the maximum capture mass-flow ratio is approached, the lowest ring total-pressure recovery occurs near the cowl surface. Referring to figure 25, the ring total-pressure distortions are relatively small at the lower capture mass-flow ratios but become large near the cowl at the higher mass-flow ratios. A low total-pressure region located in the lower right hand quadrant of the inlet (looking aft) is responsible for the large distortions. The circumferential total-pressure variation shown in figure 26 for ring number one (ring nearest the cowl) illustrates this low total-pressure region (see 160° location). Inlet distortion trends at other test Mach numbers were similar to those shown for Mach 0.9 and are not presented.

Elimination of the localized low total-pressure region would significantly improve compressor-face performance. That is, for the Mach 0.9 data shown in the lower portion of figure 26 for a total capture mass-flow ratio of 0.588, the compressor-face distortion would be reduced from 0.12 to 0.05 by elimination of the low total-pressure region. The compressor-face recovery would be increased slightly from 0.984 to 0.986.

Centerbody Fairing Effects

Limited tests were conducted with the centerbody fairing installed. Although the fairing resulted in reduced compressor-face performance, the results are not indicative of the performance to be expected for a more realistic diffuser design. Installation of the fairing further reduced the diffuser throat area in the strut region and resulted in unrealistically high diffuser Mach numbers. Redesign of the diffuser to eliminate the diffuser throat would provide lower duct Mach numbers and reduced centerbody fairing effects.

Angle-of-Attack Performance

Operation at angle of attack resulted in a slight compressor-face recovery reduction and distortion increase. The largest effect of angle of attack was to reduce the capture airflow range for stable inlet operation. Figures 27 and 28 illustrate these performance trends. The figures present compressor-face performance with the auxiliary duct fully closed ($A_{CB}/A_L = 0.0$) and for Mach numbers of 0.9 and 1.3, respectively. At Mach 0.9, the stable capture mass-flow ratio range ($\Delta W_T/W_L$) was reduced from 0.22 at zero degrees angle of attack to 0.11 at eight degrees angle of attack. At Mach 1.3, the stable capture mass-flow ratio range was reduced to zero at four degrees angle of attack. That is, at four degrees angle of attack, flow instabilities were initiated immediately upon unchoking of the main duct throat flow.

Figures 29 and 30 show that somewhat similiar performance trends were obtained with the auxiliary duct full open. However, at Mach 1.3 (figure 30), a larger stable capture airflow range was achieved. Auxiliary duct injestion of the forecone boundary layer results in a thinner centerbody boundary layer. This in turn may result in less severe shock boundary-layer interaction effects and permit operation with a greater stable capture airflow range.

Figure 31 summarizes angle-of-attack effects. The figure presents compressor-face recovery and distortion data with the auxiliary duct fully closed and fully open and for total capture mass-flow ratios of 0.52 and 0.58, respectively. The capture mass-flow ratios selected for data presentation correspond to the maximum values obtained at Mach 0.9 and eight degrees angle of attack. Although operation at lower angles of attack resulted in higher maximum capture airflows, the mass-flow ratio values selected permit performance comparison over the complete Mach number and angle-of-attack range.

Diffuser Contour

Recontouring of the inner cowl subsonic diffuser surface and the centerbody support struts is required to eliminate the diffuser second throat. Reducing the thickness of the centerbody support struts would eliminate the throat. However, strut cross-sectional area requirements for passage of centerbody bleed flows may result in a prohibitive strut length considering that the short subsonic diffuser requires the struts to penetrate the aft portion of the centerbody. Achievement of a satisfactory on-design subsonic diffuser area distribution with adequate strut passageway area probably requires lengthening of the subsonic diffuser.

COWL AUXILIARY FLOW

Subsonic Operation

Compressor-face performance. – Cowl auxiliary flow had a detrimental effect on compressor-face performance. Compressor-face recovery and distortion data illustrating this effect are presented in figure 32 for various auxiliary duct capture area ratios (A_C/A_L) and for a freestream Mach number of 0.9. The results show that a relatively small increase in total capture mass-flow ratio is accompanied by reduced recoveries and a large distortion increase. A low energy flow region near the cowl is responsible for the reduced performance as shown in figures 33 and 34 which present compressor-face rake profiles for the intermediate (A_C/A_L = 0.1) and full open (A_C/A_L = 0.2) auxiliary ducts, respectively. As discussed in a following subsection, the reduced compressor-face performance is a result of auxiliary flow injection into the main duct flow through normal holes.

Duct matching. – Back pressure limitations prevented attainment of choked auxiliary and main duct throat flows at Mach 0.9. Thus, a quantitative determination of the auxiliary and main duct choking sequence could not be made. As previously discussed, to ensure operation at a maximum capture airflow with no recovery loss due to supercritical duct flows, it is desirable that both duct throat flows choke simultaneously. Duct airflow characteristics presented in figure 35 show that, at the maximum total capture mass-flow ratio, the intermediate and full open auxiliary ducts provide auxiliary mass-flow ratios (W_C/W_L) of 0.07 and 0.11, respectively, as compared to critical values of approximately 0.1 and 0.2 assuming choked flow at the duct entrance. Inlet main duct mass-flow ratios (W_I/W_L) are 0.03 and 0.06 lower than critical for the intermediate and full open auxiliary ducts. Extrapolation of the auxiliary and main duct airflow data to critical values qualitatively indicates a proper match between the ducts for the intermediate auxiliary duct opening. The difference between critical and measured flows for the full open auxiliary duct is too great to permit assessment of the auxiliary and main duct choking sequence by data extrapolation.

Auxiliary duct entrance total-pressure recovery data presented in figure 36 shows a recovery increase with increasing auxiliary airflow. The recovery increase is due to capture of additional high energy freestream flow that would otherwise be spilled over the auxiliary door lips and a reduction in losses associated with reduced capture stream tube area divergence upstream of the auxiliary duct entrance. This latter effect is particularly apparent when comparing entrance recoveries for the full open duct with those obtained for the intermediate duct for the same auxiliary flow (fig. 36). That is, for an auxiliary mass-flow ratio (W_C/W_L) of approximately 0.08 the full open duct experiences approximately a 0.13 entrance recovery reduction. Entrance total-pressure profiles presented in figure 37 further illustrate the recovery increase with increasing auxiliary mass-flow ratio. At critical duct capture airflows, the boundary layer will occupy 40 and 20 percent of the total flow for the intermediate and full open ducts, respectively. Thus, referring to figure 37, higher entrance recoveries could be expected at critical flow rates.

The auxiliary duct plenum recoveries presented in figure 36 show that the intermediate auxiliary duct provides less airflow for the same plenum recovery than for the full open duct. This would indicate that the effective flow area through the screen is reduced for the intermediate auxiliary duct. Flow separation in the cowl auxiliary duct diffuser could result in this reduced effective flow area.

Blank-off plates. – The most pronounced effect of installing the screen blank-off plates was to further reduce compressor-face recoveries and increase distortion. Compressor-face total pressure profiles with and without the blank-off plates are presented in figure 38 for comparable auxiliary airflows and for the intermediate auxiliary duct. The results again indicate the extreme sensitivity of compressor-face performance to the interaction between the auxiliary and main duct airflows. To eliminate this interaction effect, the screen should be replaced with a flap to enable efficient merging of the auxiliary and main duct airflows. Candidate flap arrangements are described in section "Alternate Auxiliary Systems."

Supersonic Operation

At Mach 1.15, inlet performance characteristics were similar to those obtained at Mach 0.9 in that cowl auxiliary airflow had a large detrimental effect on compressor-face performance as shown in figure 39. Because of shock boundary-layer interaction effects, the total-pressure recovery of the auxiliary airflow was reduced sufficiently to result in premature choking of the main duct throat flow. Referring to figure 40, this choking sequence is evident in that the cowl auxiliary mass-flow ratio for the intermediate duct opening was considerably lower than the critical value of approximately 0.1 while choked main duct throat flow was achieved.

Comparison of the auxiliary and main duct choking characteristics obtained at Mach 0.9 (figure 35) with those obtained at Mach 1.15 (figure 40) illustrates a deficiency of a fixed exit area cowl auxiliary airflow system. Specifically, because of auxiliary airflow recovery sensitivity, simultaneous choking of auxiliary and main duct throat flows can only be achieved at the auxiliary duct design Mach number. Matching of duct choking characteristics at off-design Mach numbers would require a variable exit area auxiliary duct. Replacement of the bypass screen with a flap which deflects into the main duct airflow would provide this capability. As previously discussed, the flap arrangement would also improve compressor-face performance by efficiently merging the auxiliary and main duct airflows.

Although the centerbody auxiliary duct system employs a fixed exit area, the auxiliary and main duct choking characteristics were not sensitive to freestream Mach number. The reason for this being that, at high mass-flow ratios, the auxiliary and main duct airflow recoveries at the auxiliary duct exit station were relatively invariant with freestream Mach number (see figures 22 and 23 for $A_{CB}/A_L = 0.107$).

Compressor-face and duct performance characteristics at Mach 1.3 are presented in figures 41 and 42, respectively. The strong shock boundary-layer interaction effects further reduced auxiliary duct entrance recoveries and resulted in a greater mismatch between the auxiliary and main duct choke points.

Auxiliary duct entrance total-pressure profiles presented in figure 43 show that separated flow was present over the entire capture flow range. The separation is evident in that the total pressures near the surface are equal to the surface static pressures. The results indicate another potential problem in application of the cowl auxiliary duct system. Specifically, terminal shock induced separation at the auxiliary duct entrance would prevent attainment of full capture flow in addition to decreasing the auxiliary duct diffuser efficiency. Although a flap arrangement incorporating variable exit area capability would maximize the auxiliary flow, shock induced separation effects would not be alleviated.

Alternate Auxiliary Systems

Schematic illustrations of several alternate auxiliary cowl systems which use one or more inner flaps for efficiently merging auxiliary and main duct flows are illustrated in figure 44. Both systems provide overboard bypass capability. The simplest arrangement, arrangement A, employs a single inner flap which, in the closed position, forms the cowl inner wall surface. Upward deflection of this flap forms the auxiliary flow passage. This arrangement provides a fixed auxiliary duct exit area and would not, therefore, provide simultaneous choking of the auxiliary and main duct throat flows at critical flow rates at all off-design Mach numbers. Arrangement B provides a variable duct exit area capability through addition of a second inner flap. This arrangement would provide matching at off-design Mach numbers. Both arrangements may require a lengthened subsonic diffuser. Specifically, the close proximity of the auxiliary duct exit to the main duct geometric throat (on-design centerbody position) may not provide sufficient space for ducting of cowl throat boundary-layer bleed flows.

CONCLUDING REMARKS

An experimental evaluation of an approximately 1/3 scale model of a Mach 2.65 axisymmetric mixed-compression inlet with centerbody and cowl auxiliary airflow systems was conducted. The evaluation was conducted in the NASA Ames 11-by 11-ft Unitary Plan Wind Tunnel Facility at Mach numbers ranging from 0.6 to 1.3.

At a 0.1 total-pressure distortion level, the centerbody auxiliary airflow system provided a total capture mass-flow ratio increase of 0.055 and 0.051 and a total-pressure recovery increase of 0.015 and 0.012 at Mach 0.9 and 1.3, respectively. A geometric throat just upstream of the compressor face limited the total capture mass-flow ratio increase to less than the desired critical value of approximately 0.11. Operation of the centerbody auxiliary system resulted in main duct flow separation on the centerbody. This separation reduced the effective main duct flow area at the auxiliary duct exit station and permitted choking of the auxiliary duct throat flow prior to choking of the main duct throat flow. Premature choking of the auxiliary duct results in supercritical duct flow with excessive total-pressure recovery losses prior to attainment of the maximum capture airflow.

Future work should include recontouring of the inner cowl subsonic diffuser surface and the centerbody support struts to eliminate the diffuser second throat. Reducing the thickness of the centerbody support struts would eliminate the throat. However, strut cross-sectional area requirements for passage of centerbody bleed flows may result in a prohibitive strut length considering that the short diffuser requires the struts to penetrate the aft centerbody skirt. Achievement of a satisfactory on-design subsonic diffuser area distribution may also require lengthening of the subsonic diffuser.

Cowl auxiliary flow had a large detrimental effect on compressor-face performance. Auxiliary airflow passage through the porous bypass screen and subsequent interaction with the main duct airflow was responsible for the reduced performance. Operation at subsonic Mach numbers resulted in simultaneous choking of auxiliary and main duct throat flows. However, at supersonic speeds, shock boundary-layer interaction effects upstream of the auxiliary duct entrance sufficiently reduced the auxiliary flow total-pressure recovery to result in premature choking of the

main duct throat flow. Strong shock boundary-layer interaction effects may prevent attainment of critical duct airflows at Mach 1.3.

Replacement of the bypass screen with a flap arrangement is recommended to obtain efficient merging of auxiliary and main duct flows. A flap arrangement would also allow variation of auxiliary duct exit area to obtain similar auxiliary and main duct choking characteristics over a range of transonic Mach numbers.

Excellent on-design (centerbody retracted to Mach 2.65 position) subsonic diffuser performance was achieved when operating with a throat Mach number of approximately 0.8 (representative of Mach number downstream of throat terminal shock wave when operating at Mach 2.65.) A high subsonic diffuser total-pressure recovery of 0.965 and a compressor-face total-pressure distortion of approximately 0.1 was achieved with the centerbody fairing installed and the cowl and centerbody vortex generators removed. Removal of the centerbody fairing decreased the diffuser total-pressure recovery by 0.005 and increased compressor-face distortion by 0.02. Although the centerbody vortex generators did not degrade the diffuser performance, installation of the cowl vortex generators resulted in a 0.04 total-pressure recovery loss and increased distortion. These on-design performance results may be representative of the subsonic diffuser performance to be expected when operating at Mach 2.65 provided that the terminal shock is near the throat (operation at critical point) and that sufficient boundary layer bleed is used to prevent boundary-layer separation downstream of the terminal shock boundary-layer interaction.

REFERENCES

1. Boeing Commercial Airplane Company: Advanced Supersonic Configurations Studies Using Multicycle Engines for Civil Aircraft. NASA CR-132723, September 1975.

2. Douglas Aircraft Company: Technology Application Studies for Supersonic Cruise Aircraft. NASA CR-144925, November 1975.

3. Wright, B. R.; Foss, R. L.; Benson, J. L.; and Byrnes, A. L.: Technology Assessment Studies Applied to Supersonic Cruise Vehicles. NASA CR-144916, October 1975.

4. Syberg, J.; and Koncsek, J. L.: Transonic and Supersonic Test of the SST Prototype Air Intake. FAA-55-72-50, April 1972.

5. Koncsek, J. L.; and Syberg, J.: Transonic and Supersonic Test of a Mach 2.65 Mixed-Compression Axisymmetric Intake. NASA CR 1977, March 1972.

6. Sorensen, Norman E.; Latham, Eldon A.; and Smeltzer, Donald B.; Variable Geometry for Mixed-Compression Inlets. AIAA Paper No. 74-1172, October 1974.

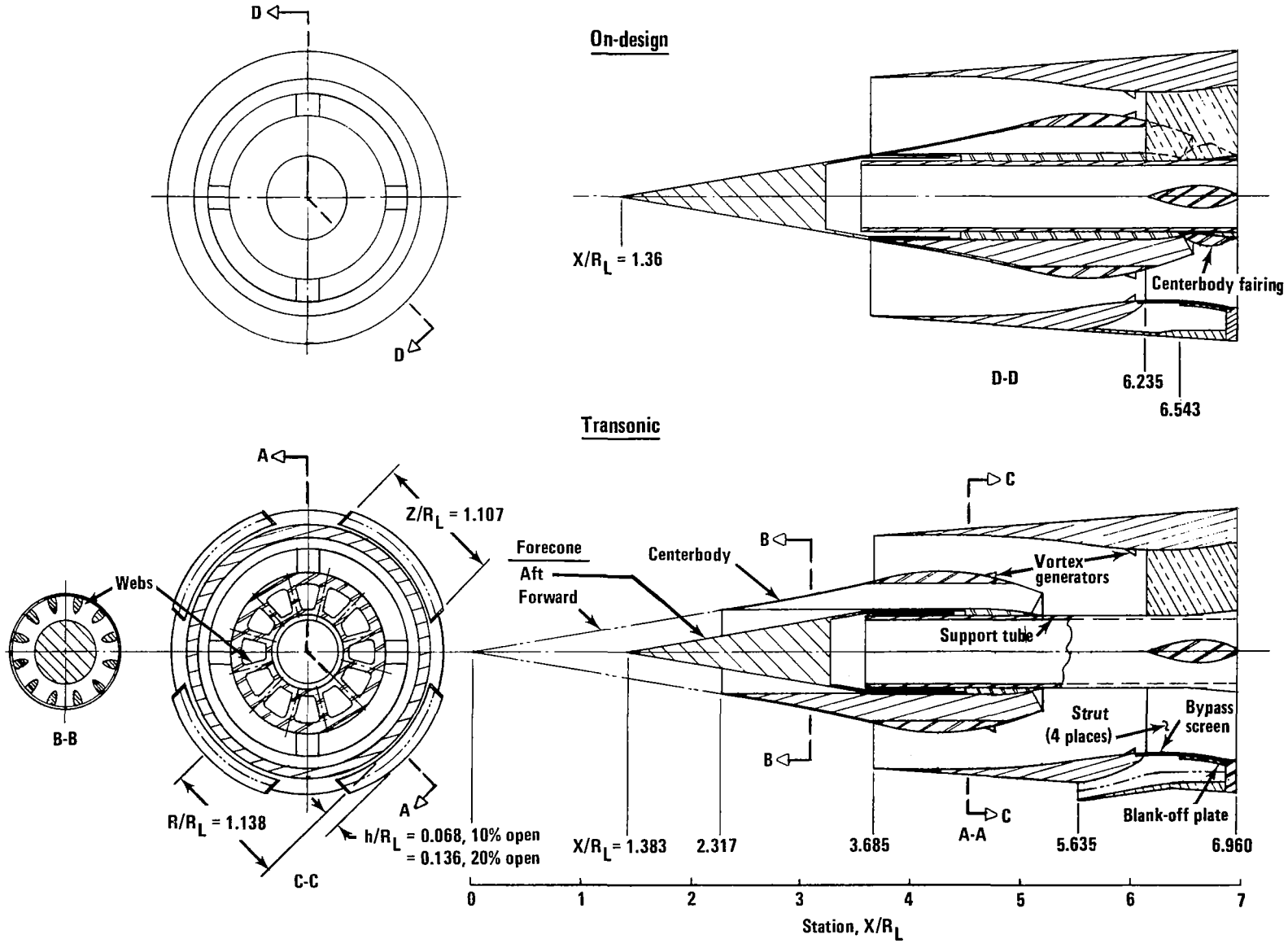

Figure 1.–Model Schematic

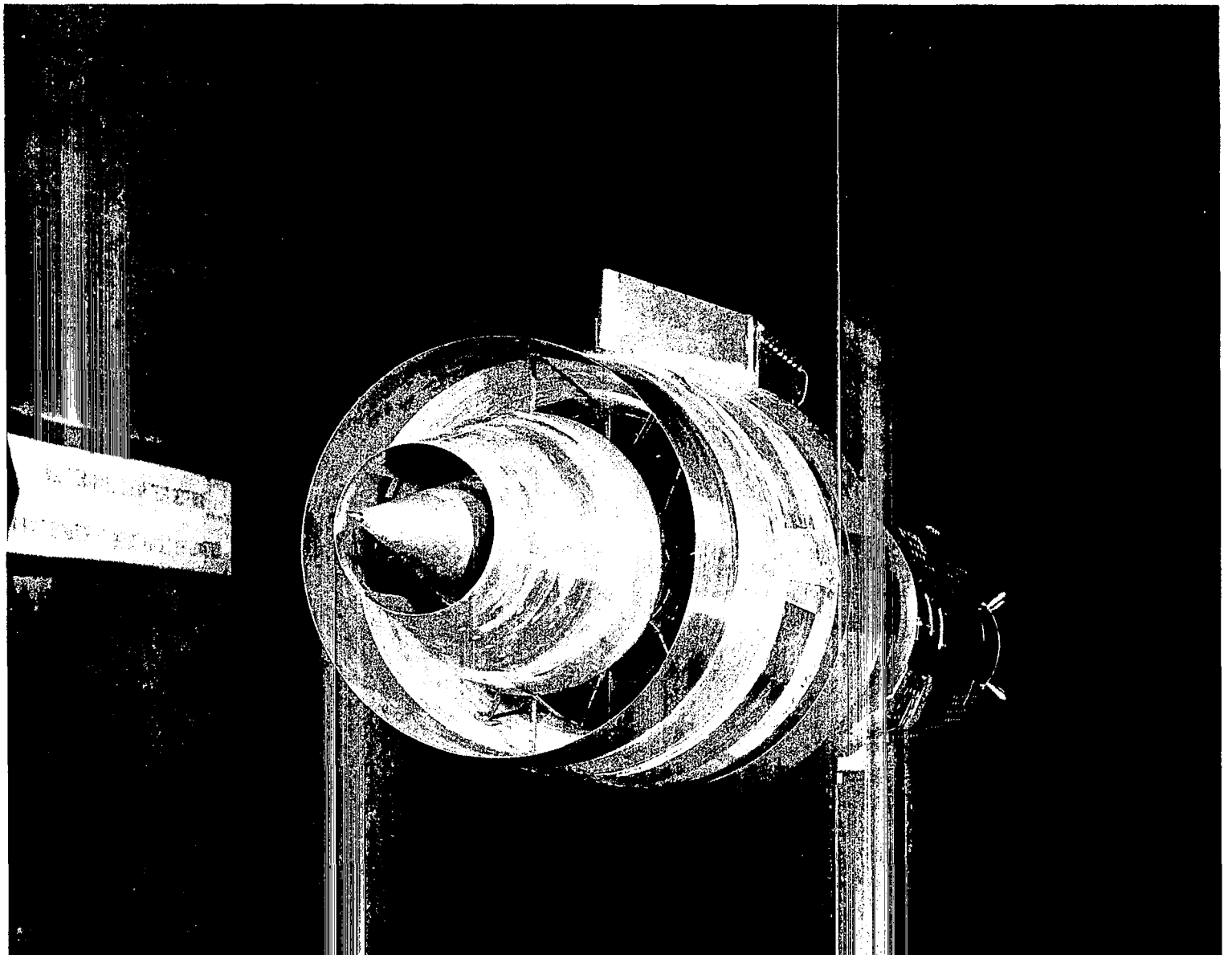

Figure 2.–Model with Centerbody Auxiliary Duct Fully Open

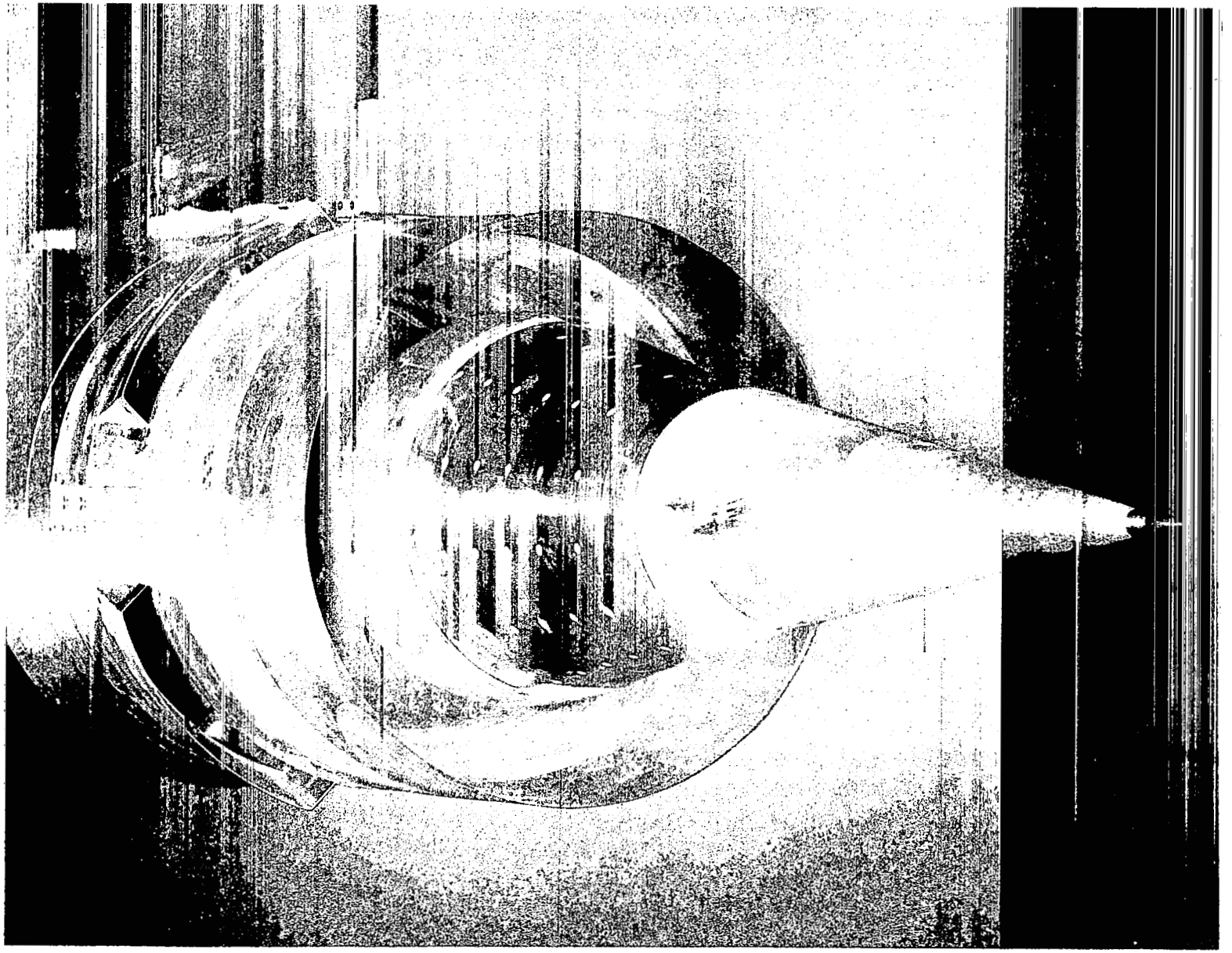

Figure 3.–Model with Cowl Auxiliary Scoops Fully Open

Location	Station X/R_L	h/R_L	ℓ/R_L	Spacing a/b
Cowl	6.11	0.03	0.06	2
Centerbody	6.06 (on design)	0.05	0.10	2

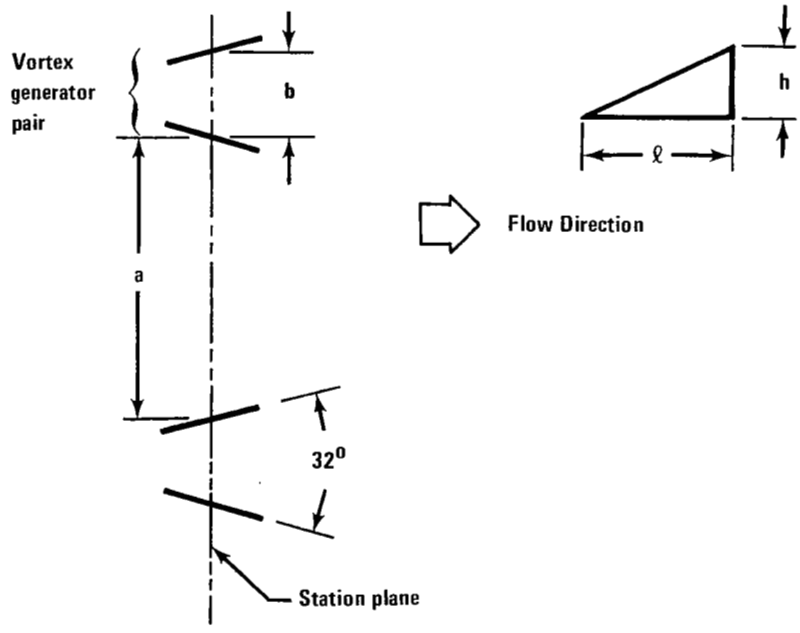

Figure 4.–Vortex Generator Arrangement

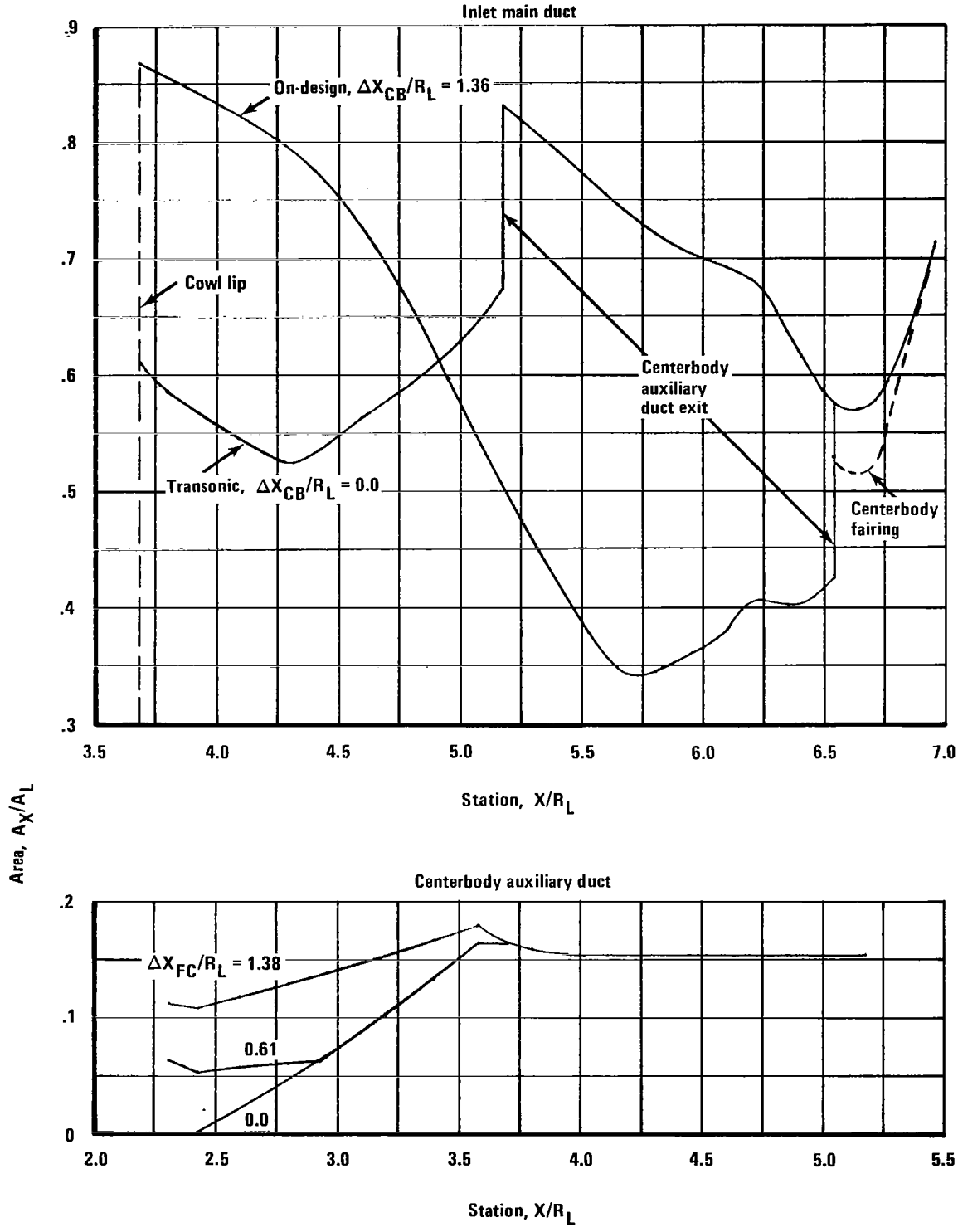

Figure 5.—Inlet Area Distributions

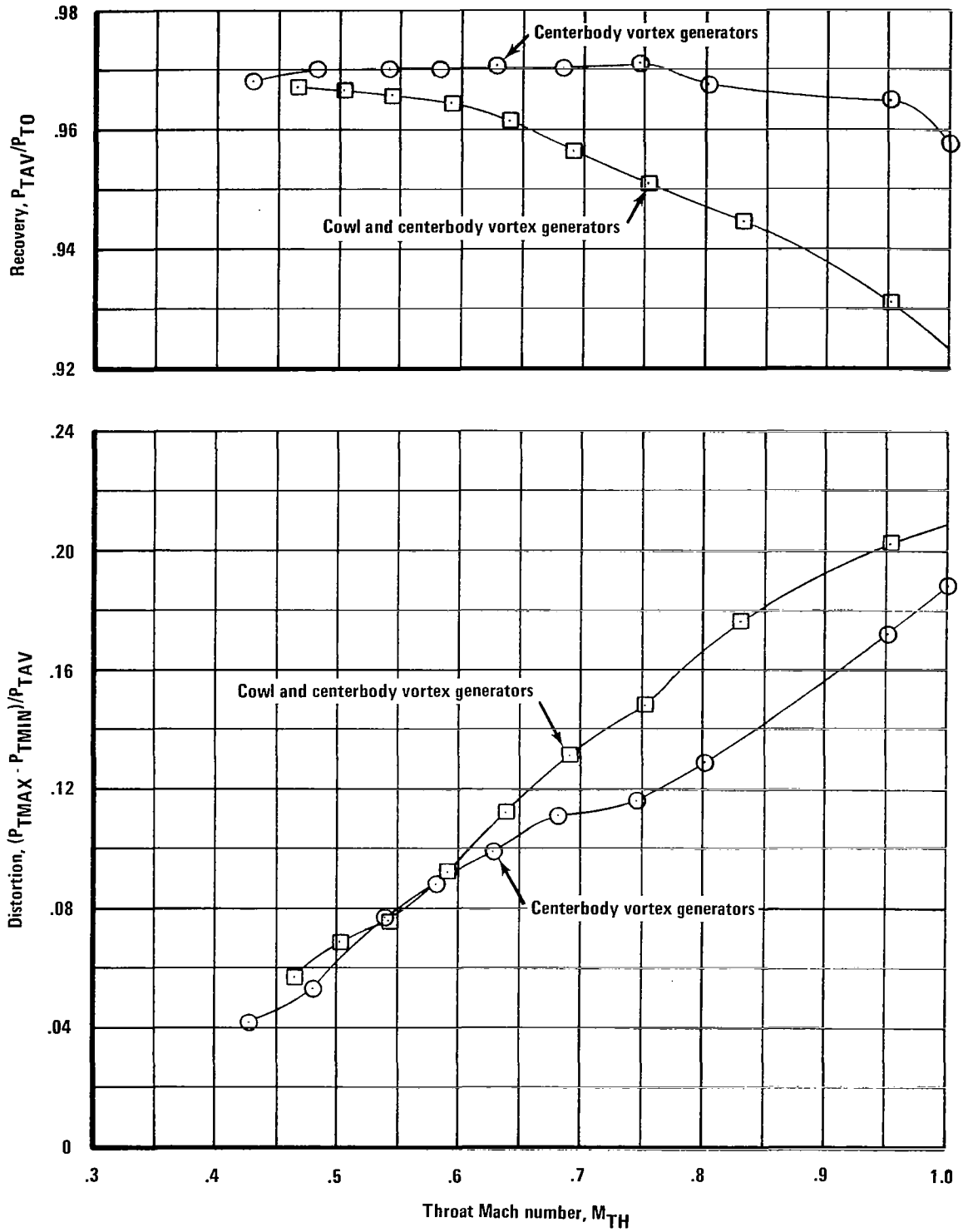

Figure 6.–Effect of Cowl Vortex Generators on Diffuser On-Design Performance, $M_L = 0.9$, Centerbody Fairing Removed

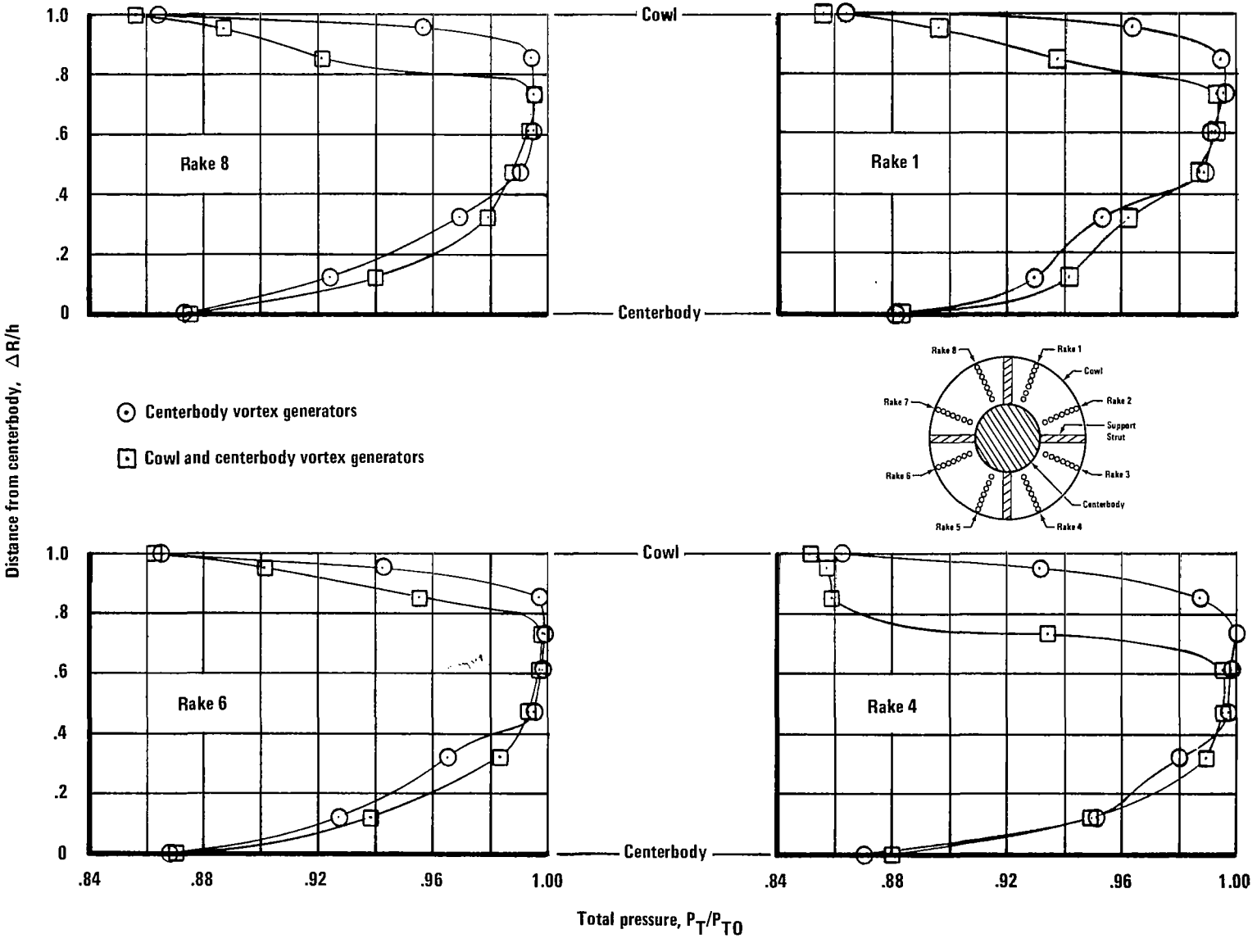

Figure 7.–Effect of Cowl Vortex Generators on Compressor-Face Total-Pressure Profiles, $M_L = 0.9$, $M_{TH} = 0.75$, Centerbody Fairing Removed

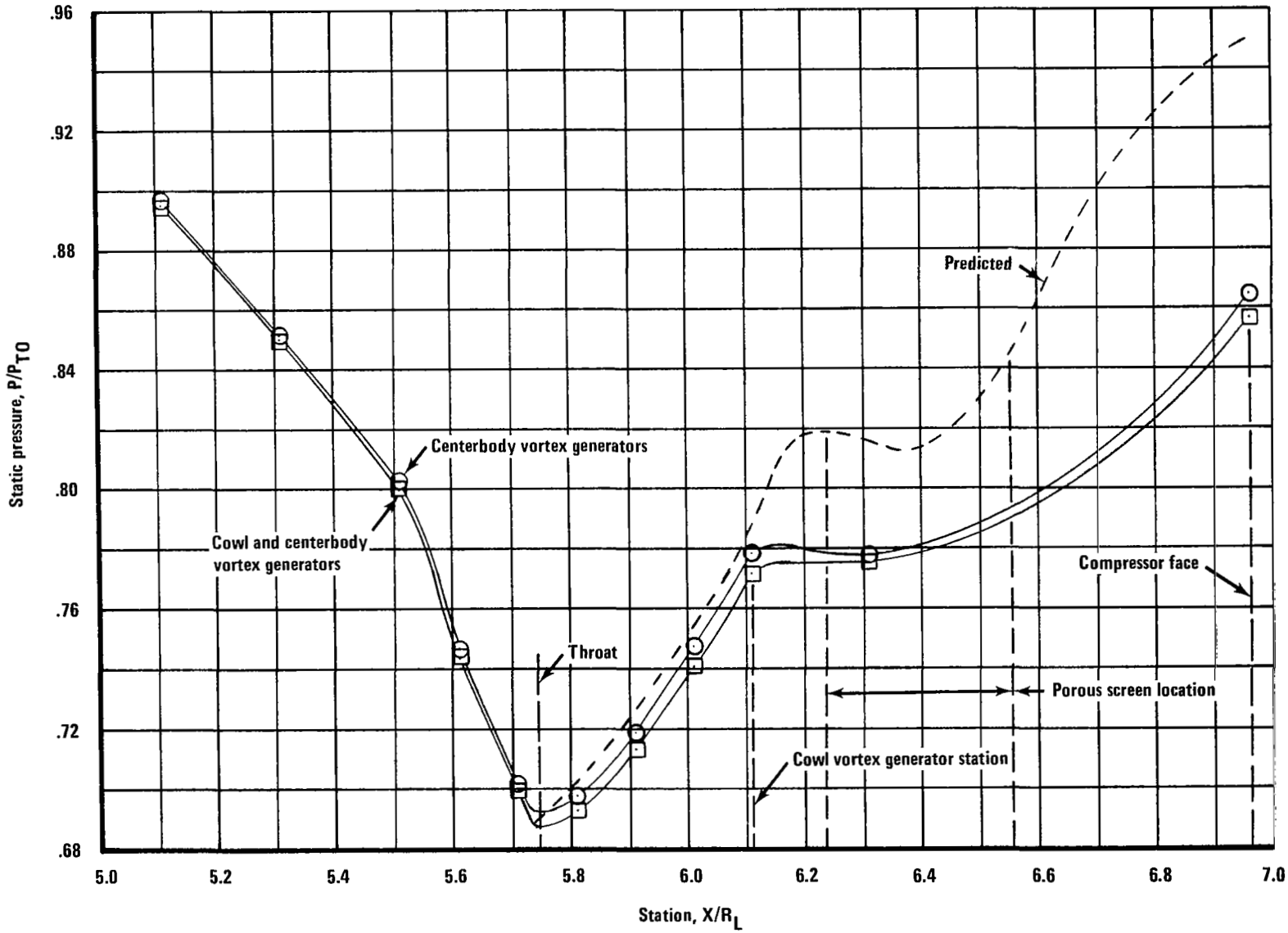

Figure 8.–Effect of Cowl Vortex Generators on Cowl Static Pressure Distributions, $M_L = 0.9$, $M_{TH} = 0.75$, Centerbody Fairing Removed

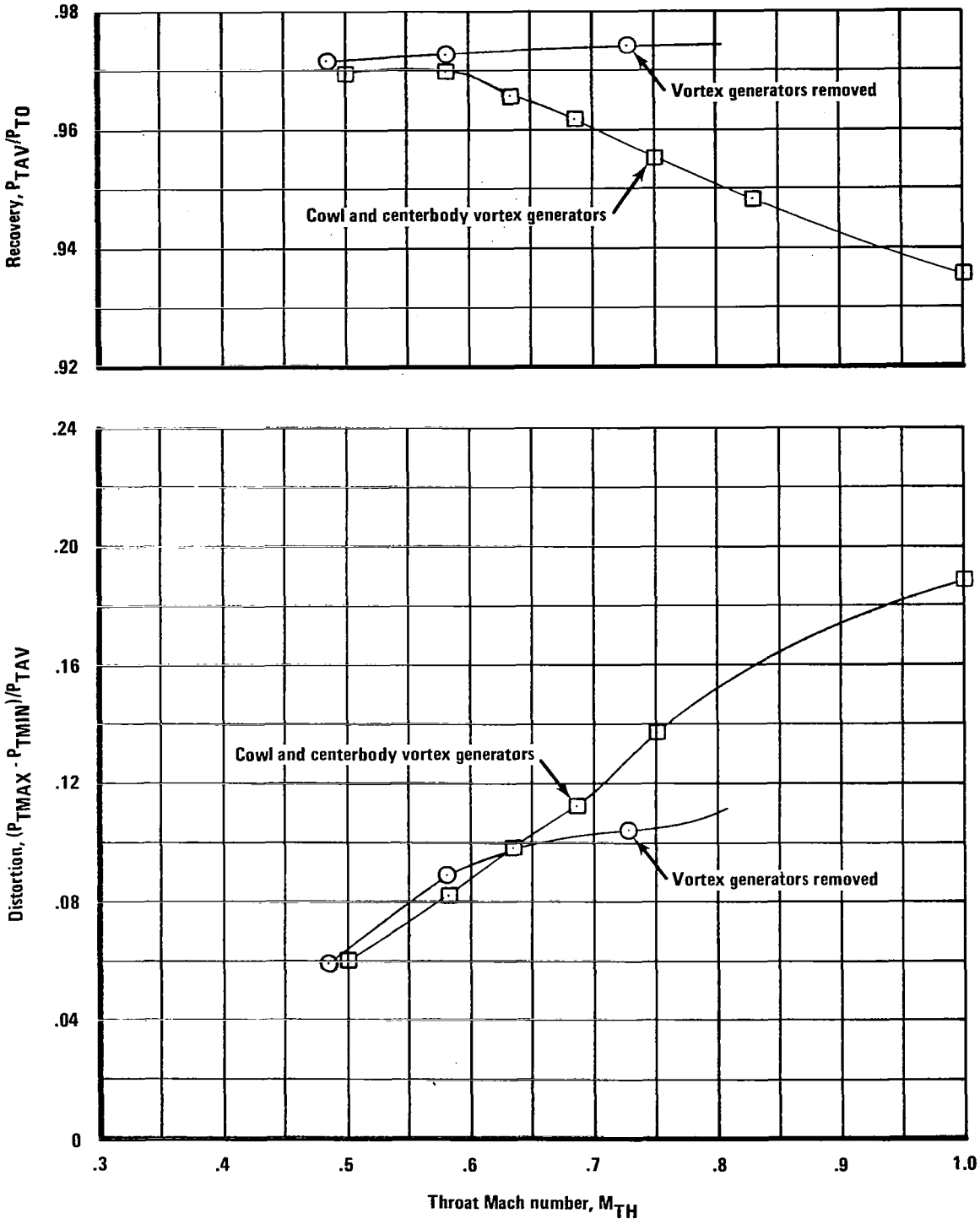

Figure 9.–Effect of Cowl and Centerbody Vortex Generators on Diffuser On-Design Performance, $M_L = 0.9$, Centerbody Fairing Installed

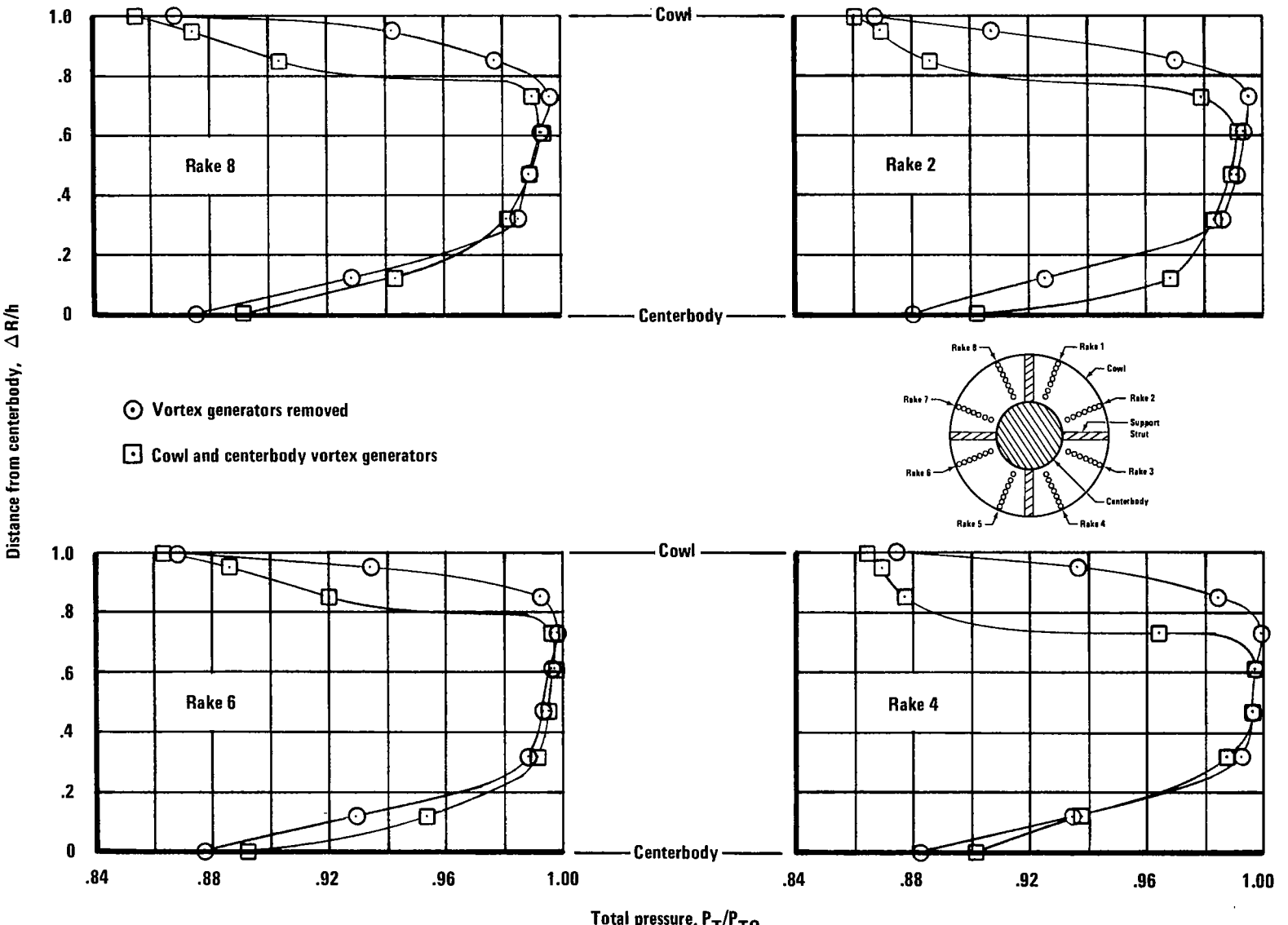

Figure 10.–Effect of Cowl and Centerbody Vortex Generator on Compressor-Face Total-Pressure Profiles, $M_L = 0.9$, $M_{TH} = 0.75$, Centerbody Fairing Installed

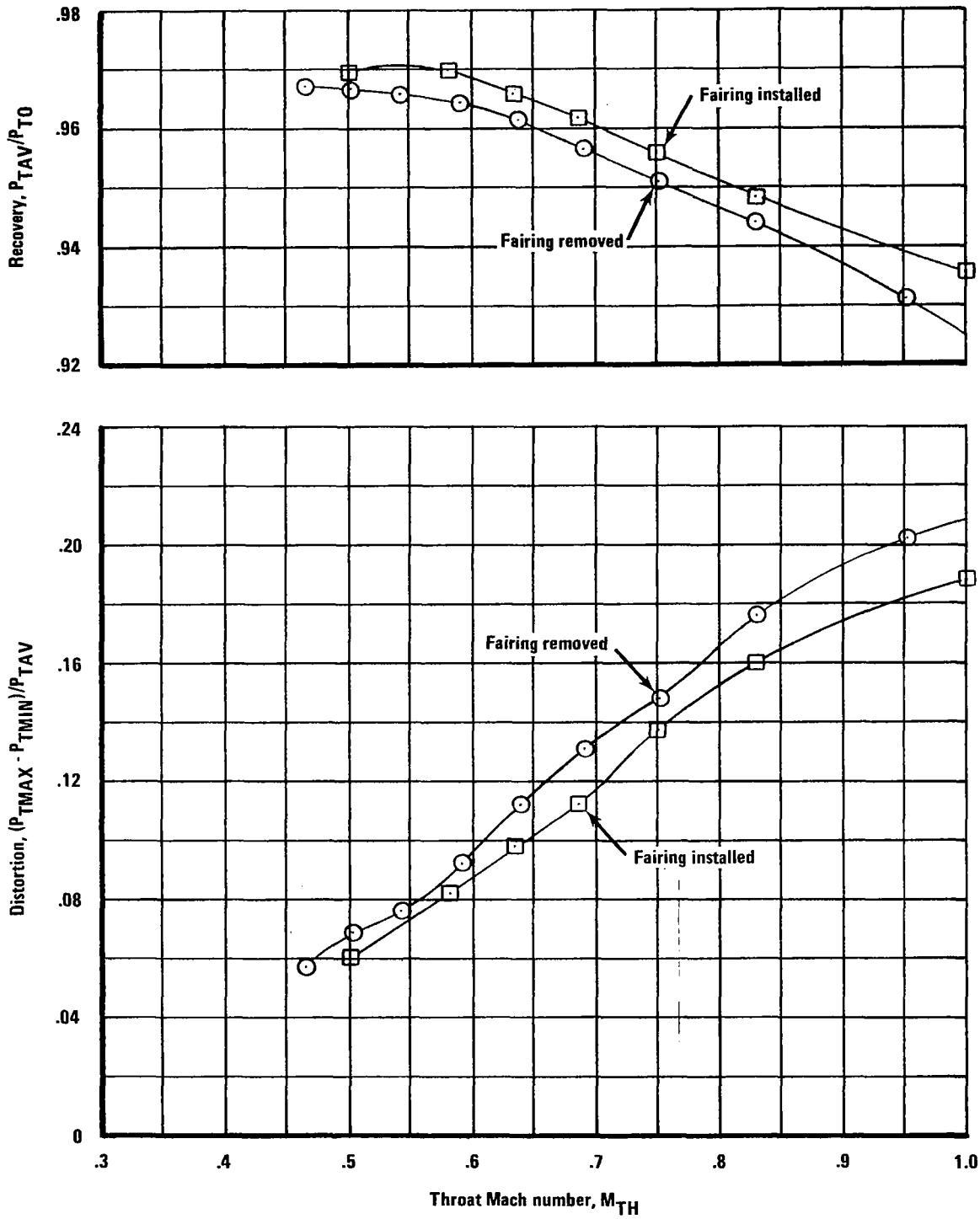

Figure 11.–Effect of Centerbody Aft Fairing on Diffuser On-Design Performance, $M_L = 0.9$

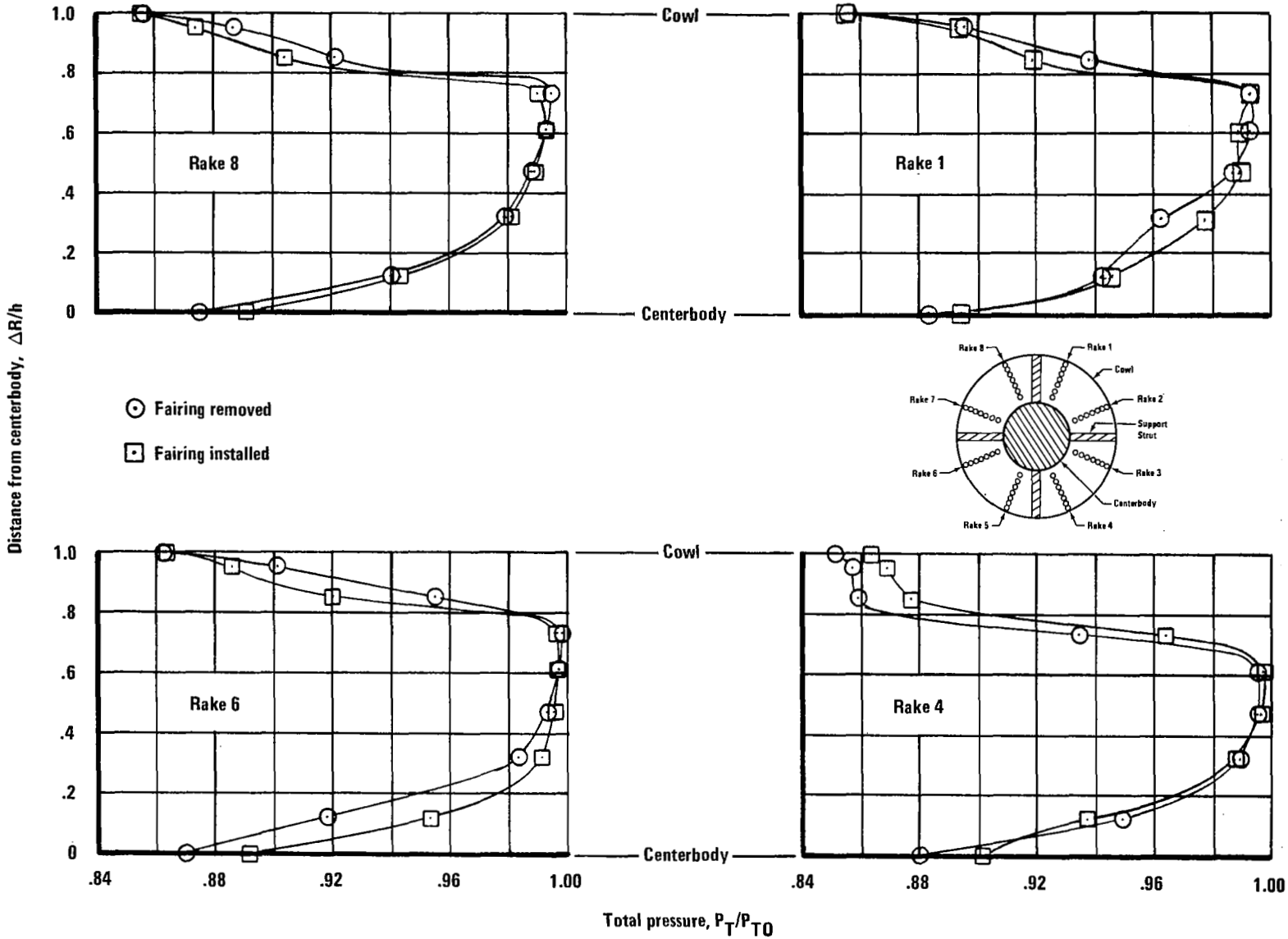

Figure 12.–Effect of Centerbody Aft Fairing on Compressor-Face Total-Pressure Profiles, $M_L = 0.9$, $M_{TH} = 0.75$

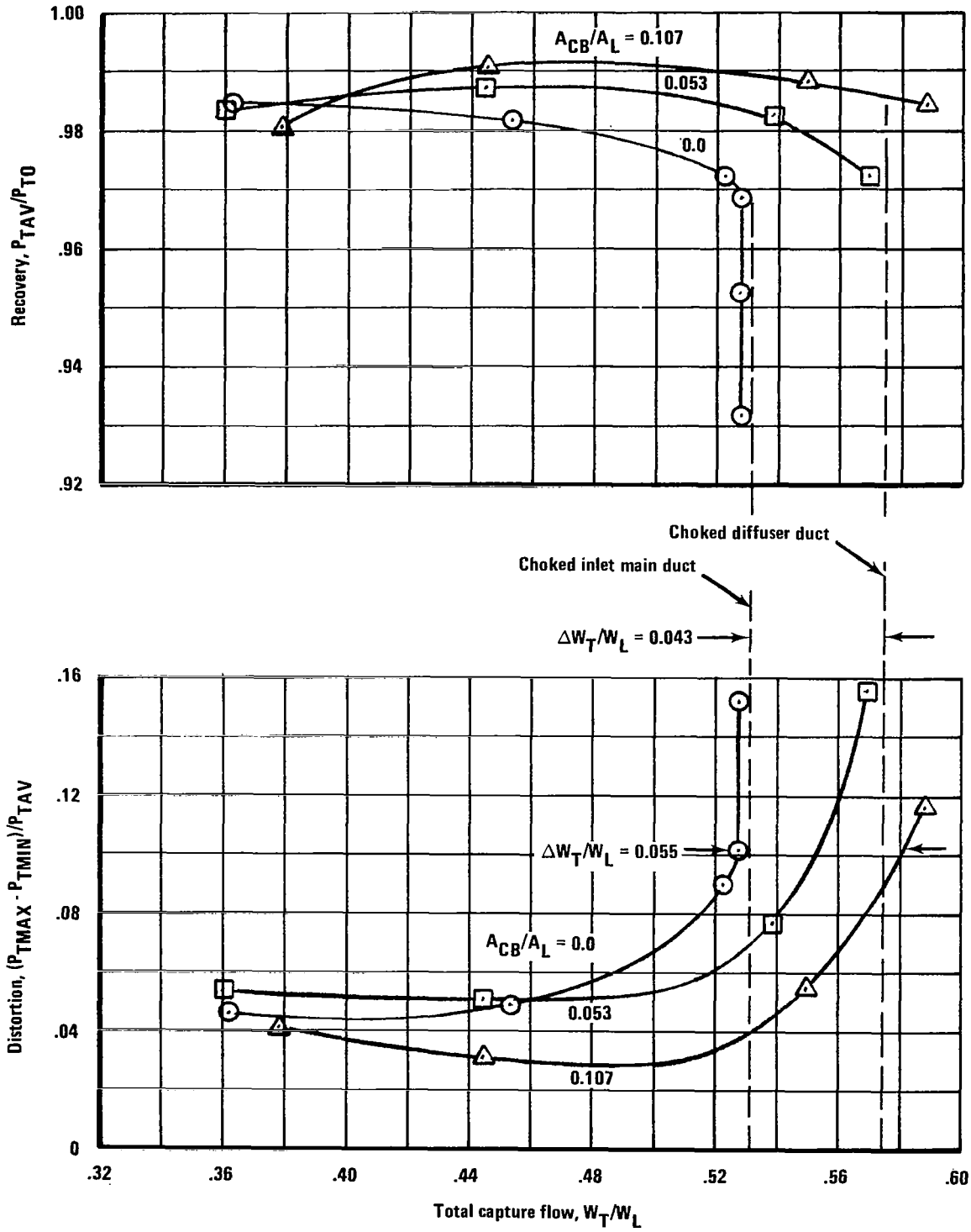

Figure 13.–Intake Performance with Centerbody Auxiliary Flow, M_L = 0.9

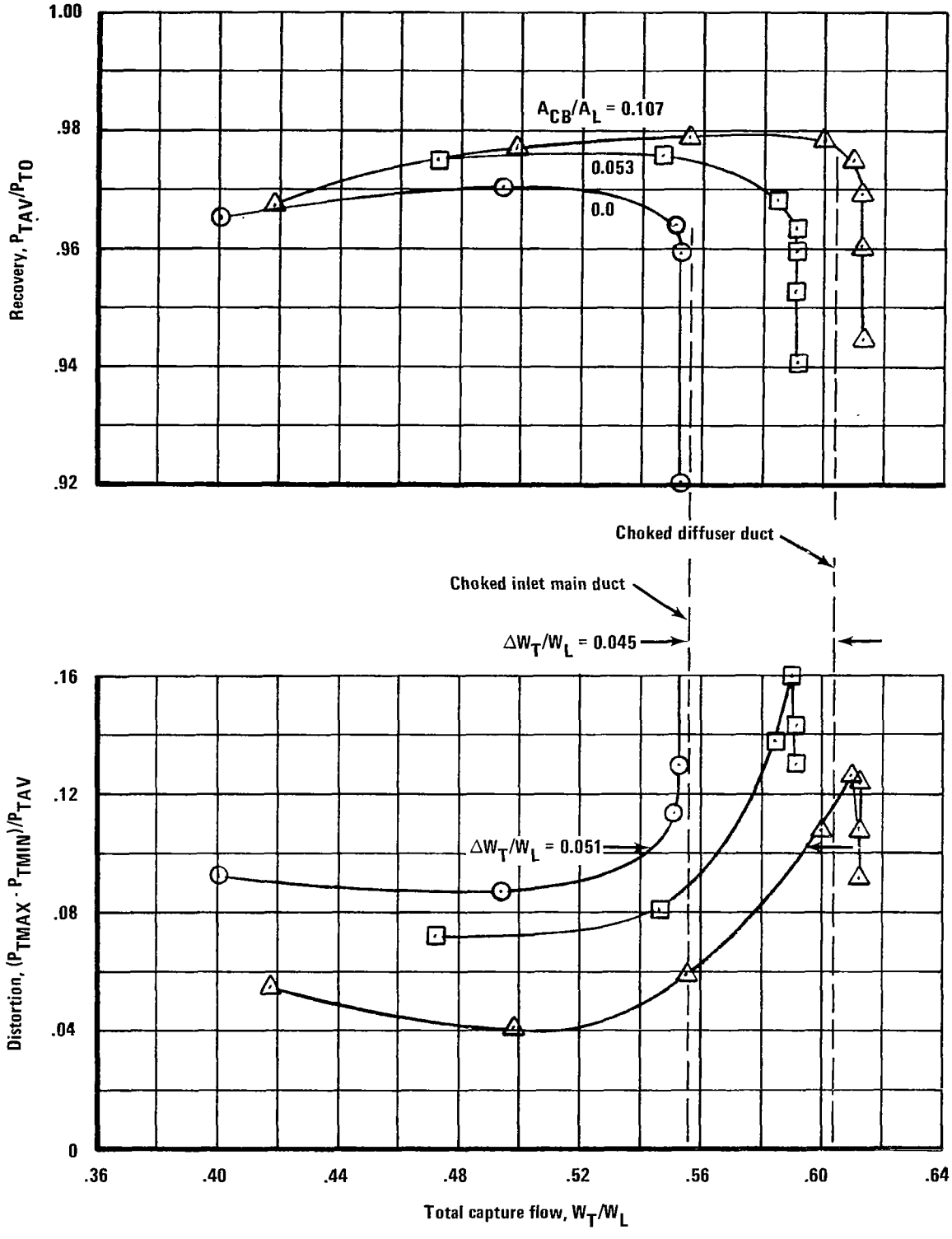

Figure 14.—Intake Performance with Centerbody Auxiliary Flow, M_L = 1.3

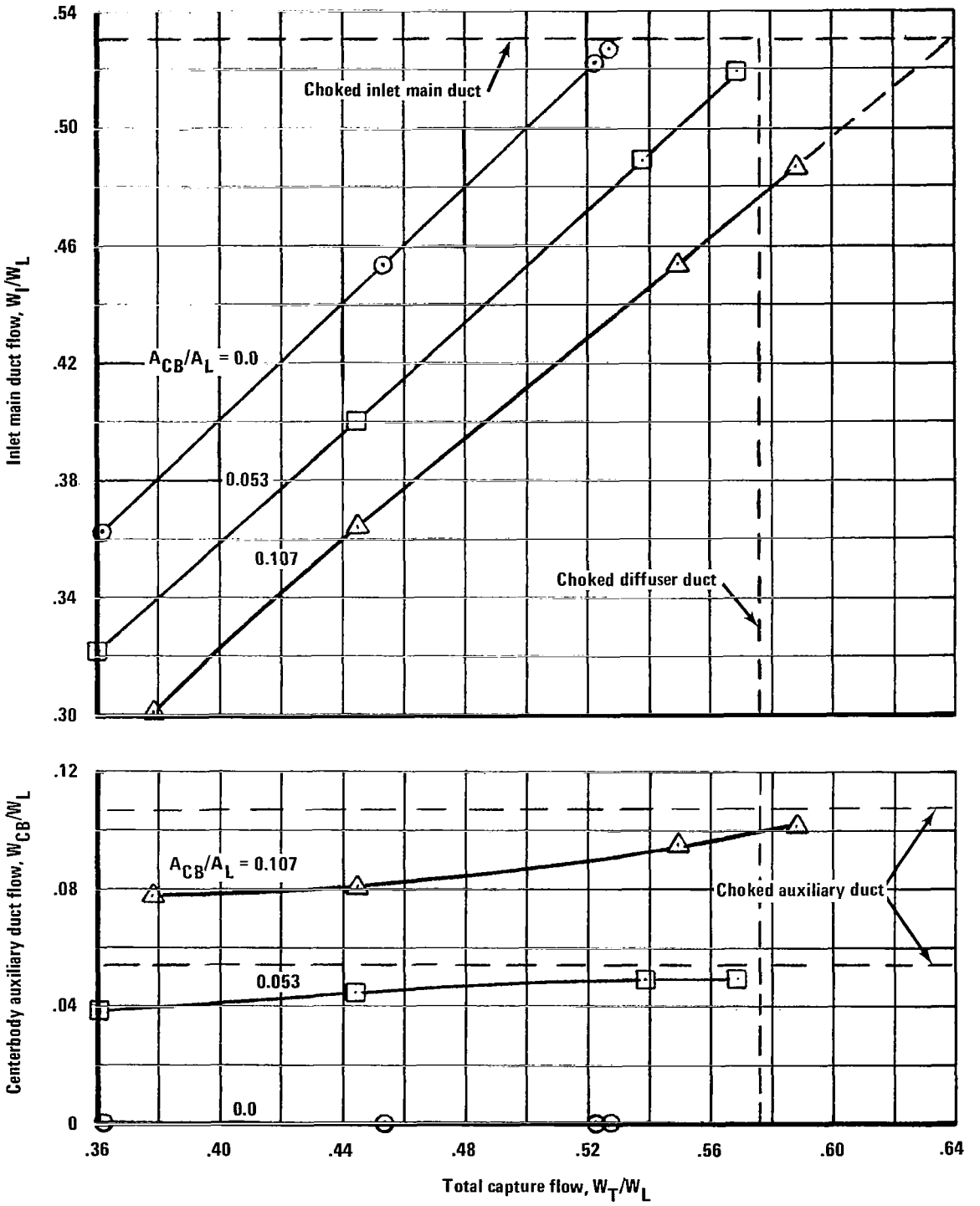

Figure 15.–Inlet/Centerbody-Auxiliary-Duct Flow Characteristics, M_L = 0.9

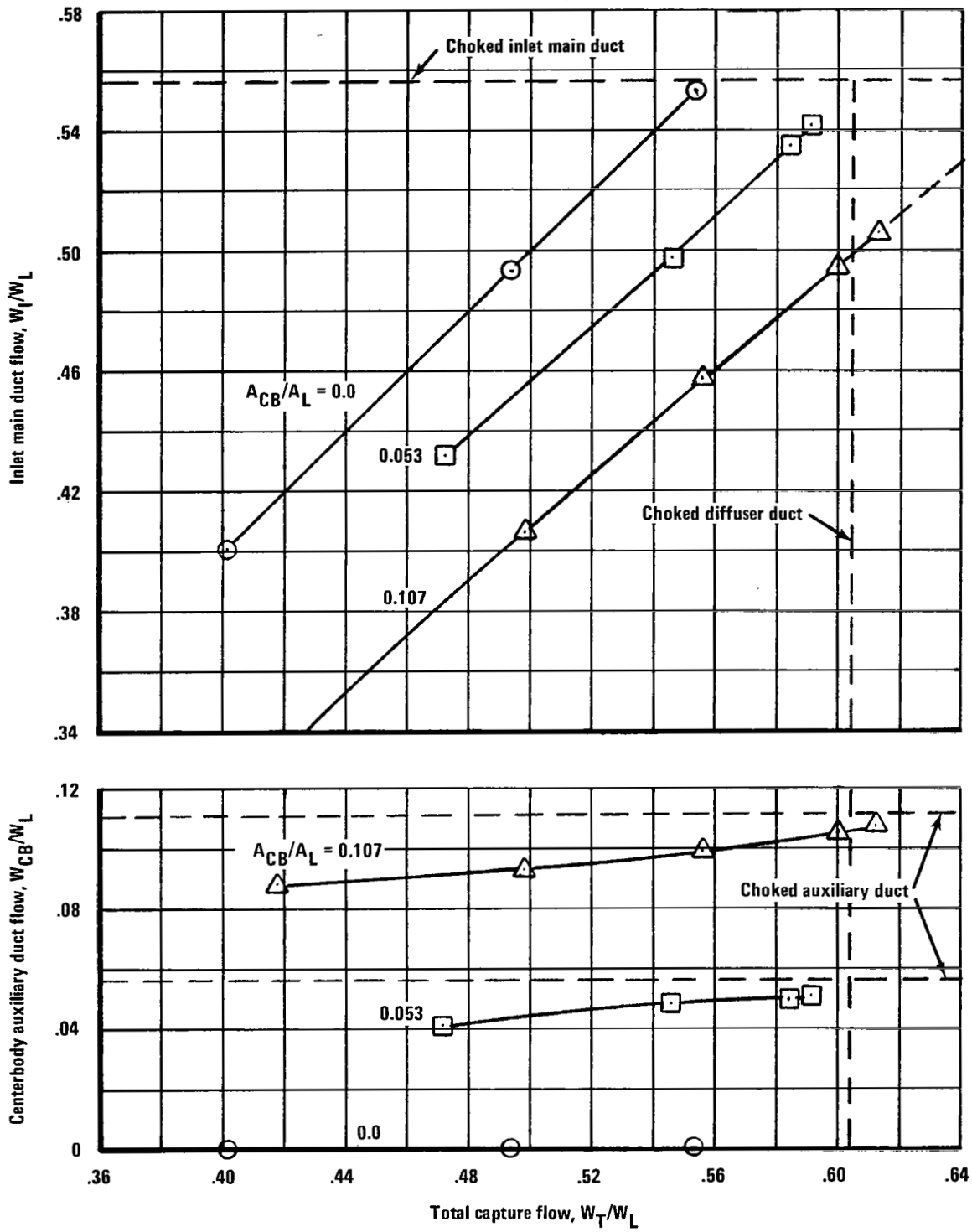

Figure 16.—Inlet/Centerbody-Auxiliary-Duct Flow Characteristics, $M_L = 1.3$

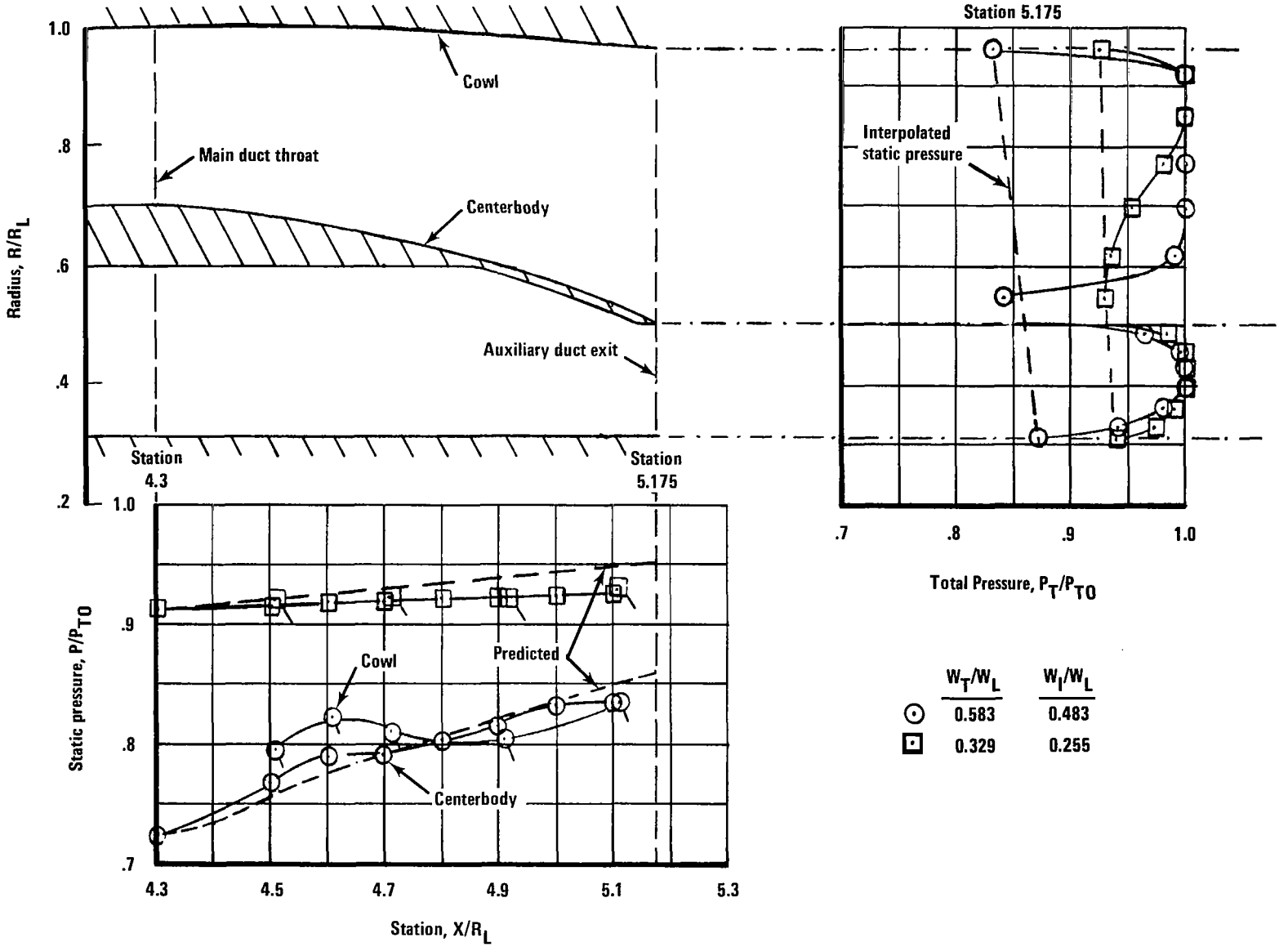

Figure 17.–Diffuser Pressure Distributions and Exit Recovery Profiles at $X/R_L = 5.175$, $M_L = 0.9$, $A_{CB}/A_L = 0.107$

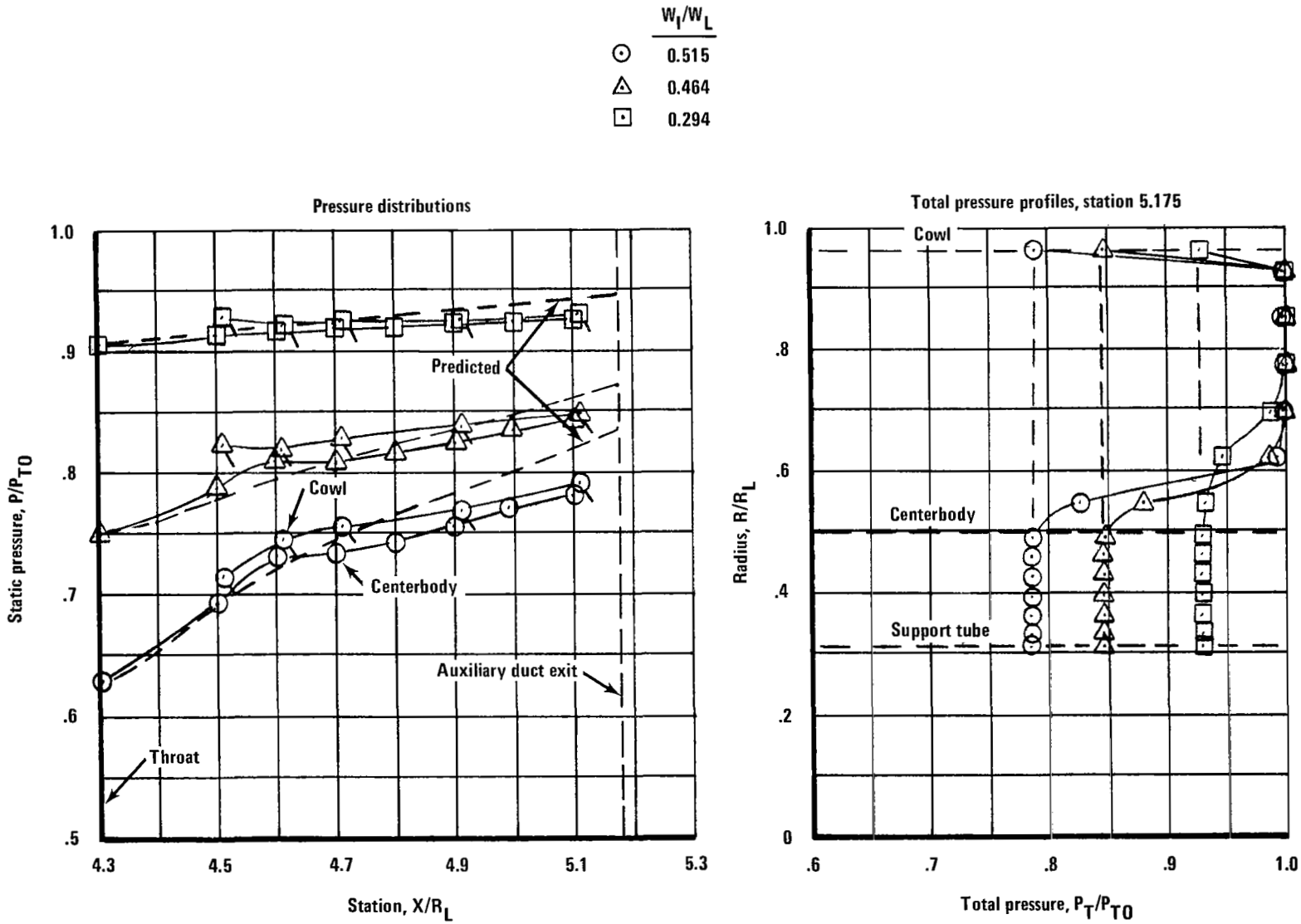

Figure 18.–Diffuser Pressure Distributions and Exit Recovery Profiles at $X/R_L = 5.175$, $M_L = 0.9$, $A_{CB}/A_L = 0$

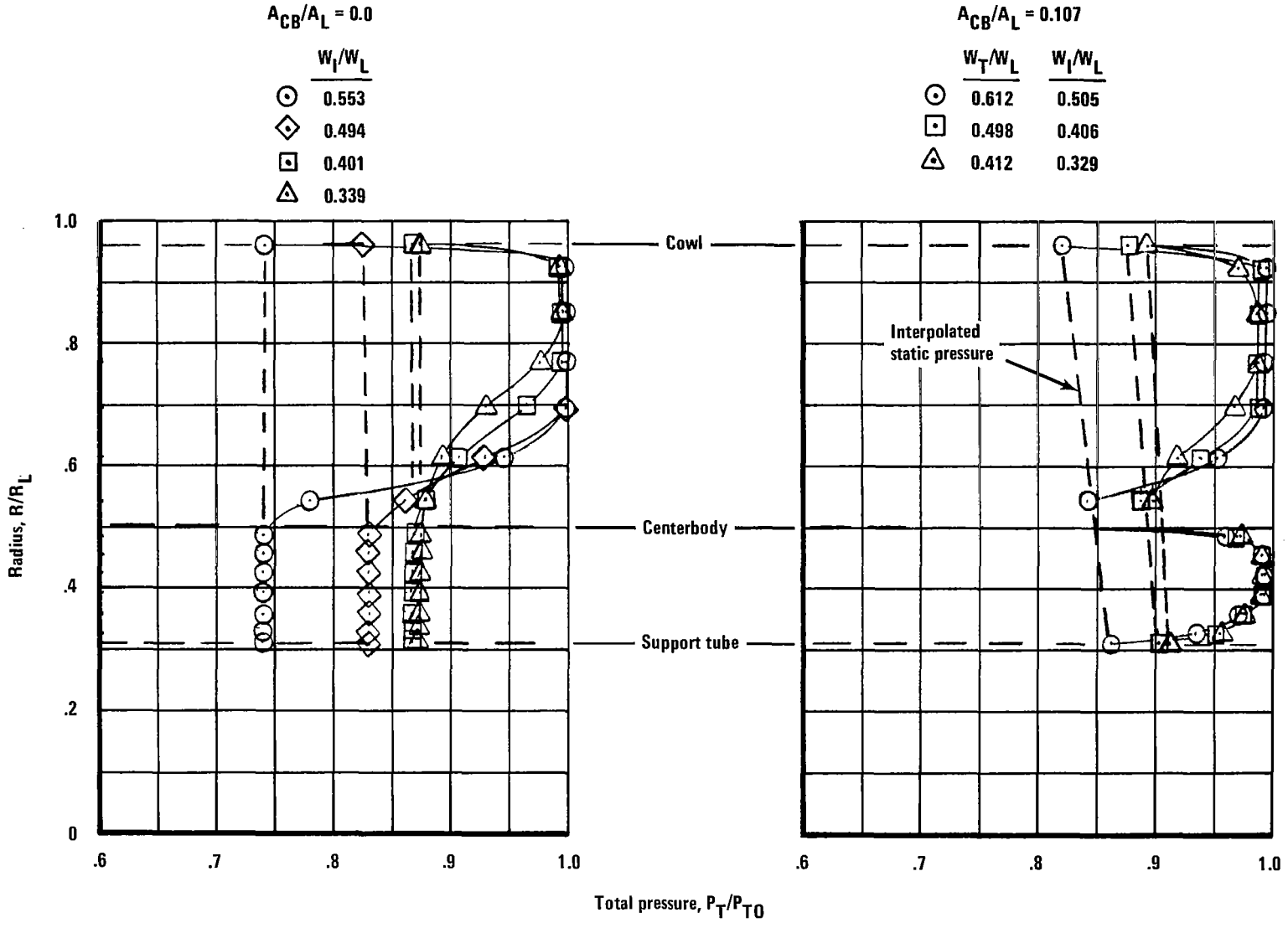

Figure 19.–Inlet/Auxiliary-Duct Recovery Profiles at X/R_L = 5.175, M_L = 1.3

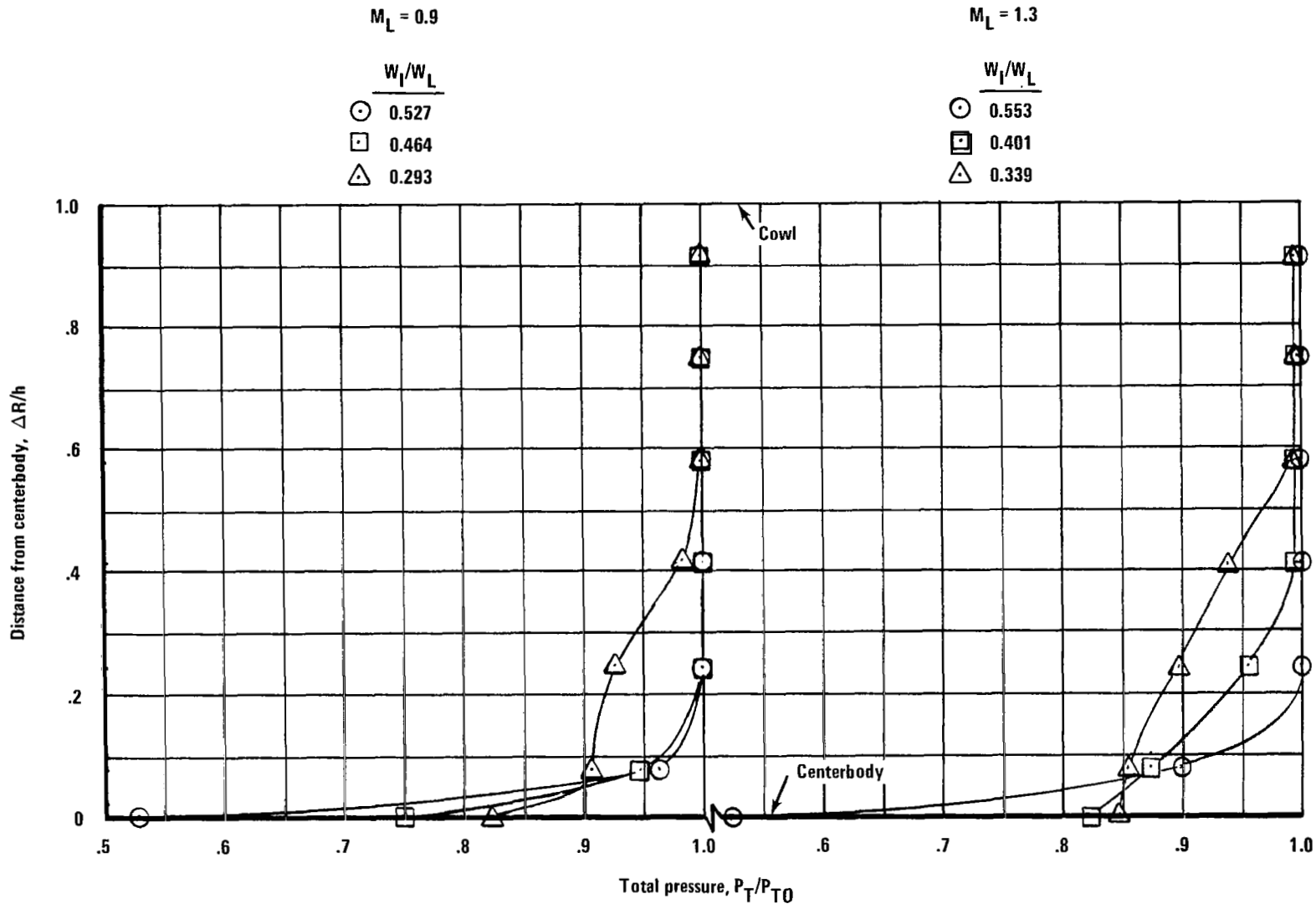

Figure 20.—Inlet Main Duct Throat Total-Pressure Profiles, $A_{CB}/A_L = 0$

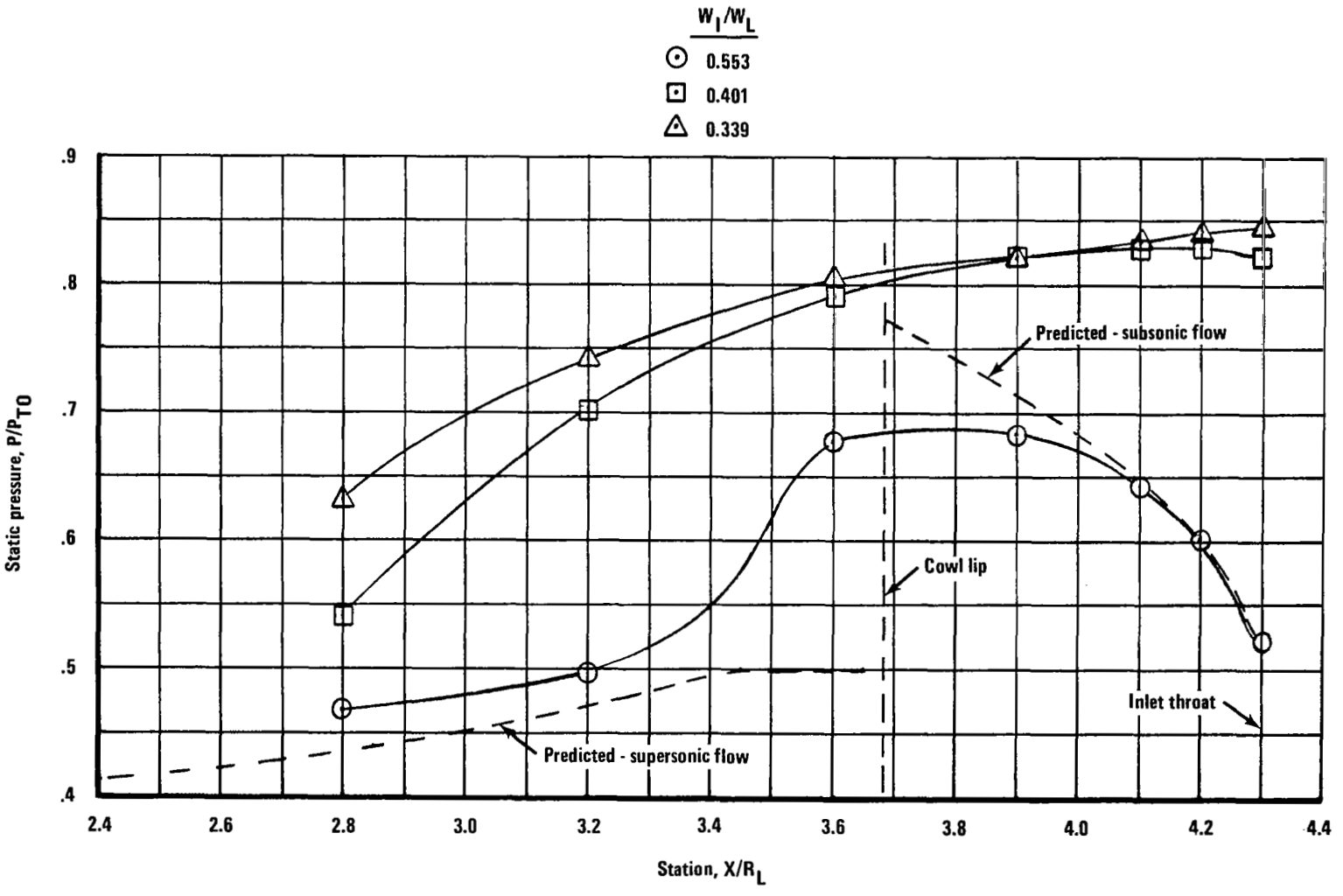

Figure 21.–Supersonic Diffuser Centerbody Pressure Distributions, Mach 1.3, $A_{CB}/A_L = 0$

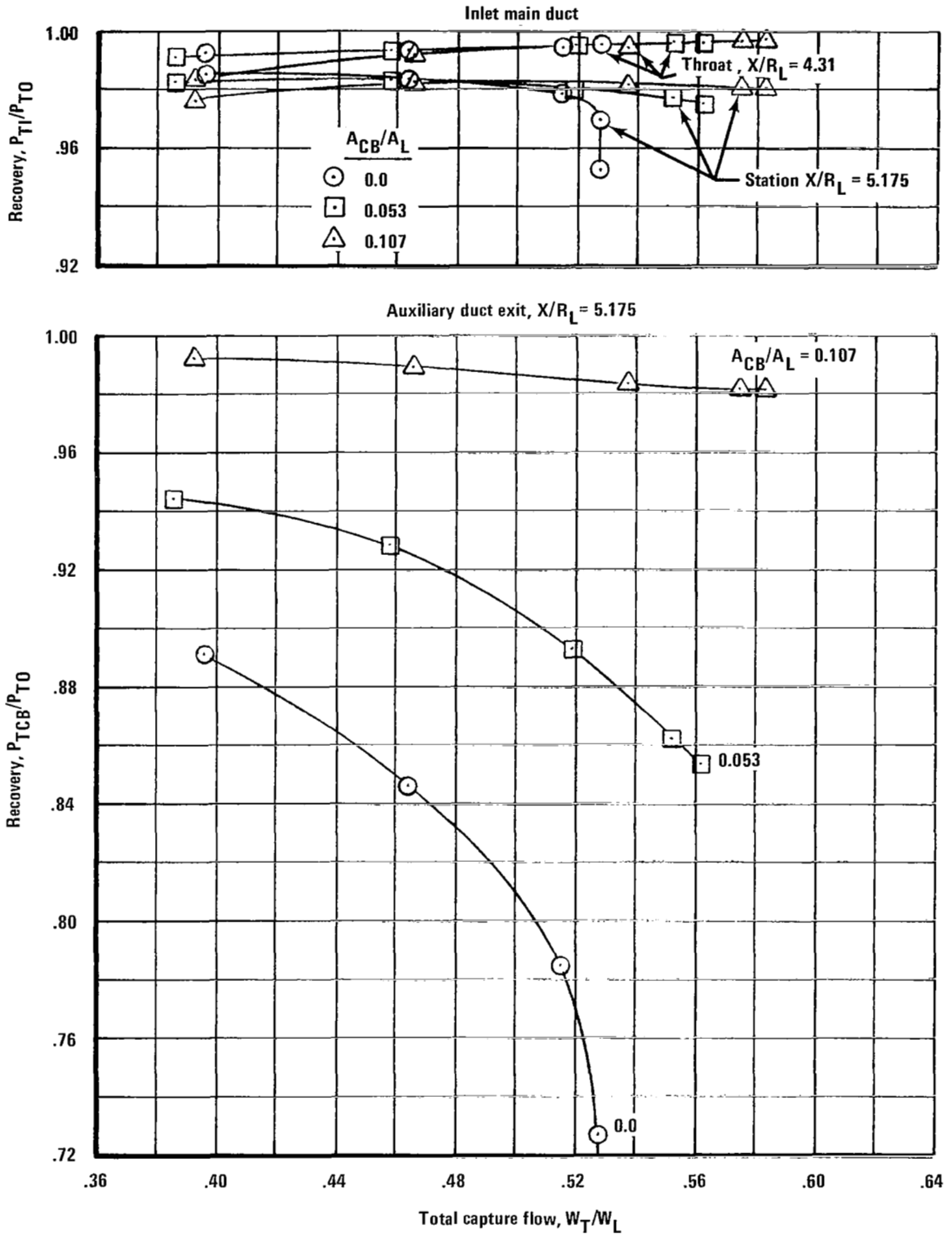

Figure 22.–Inlet/Centerbody-Auxiliary-Duct Recovery Characteristics, $M_L = 0.9$

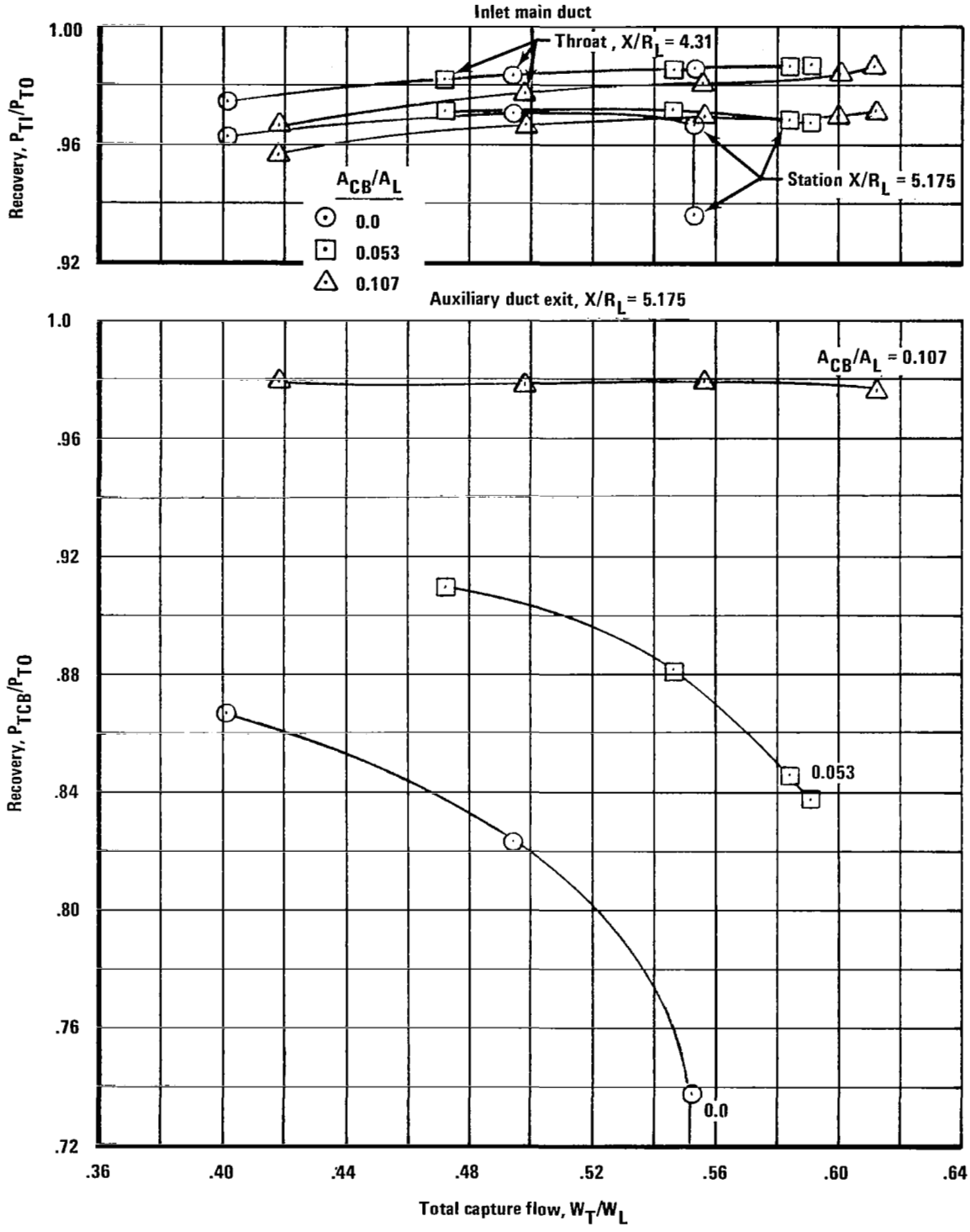

Figure 23.–Inlet/Centerbody-Auxiliary-Duct Recovery Characteristics, $M_L = 1.3$

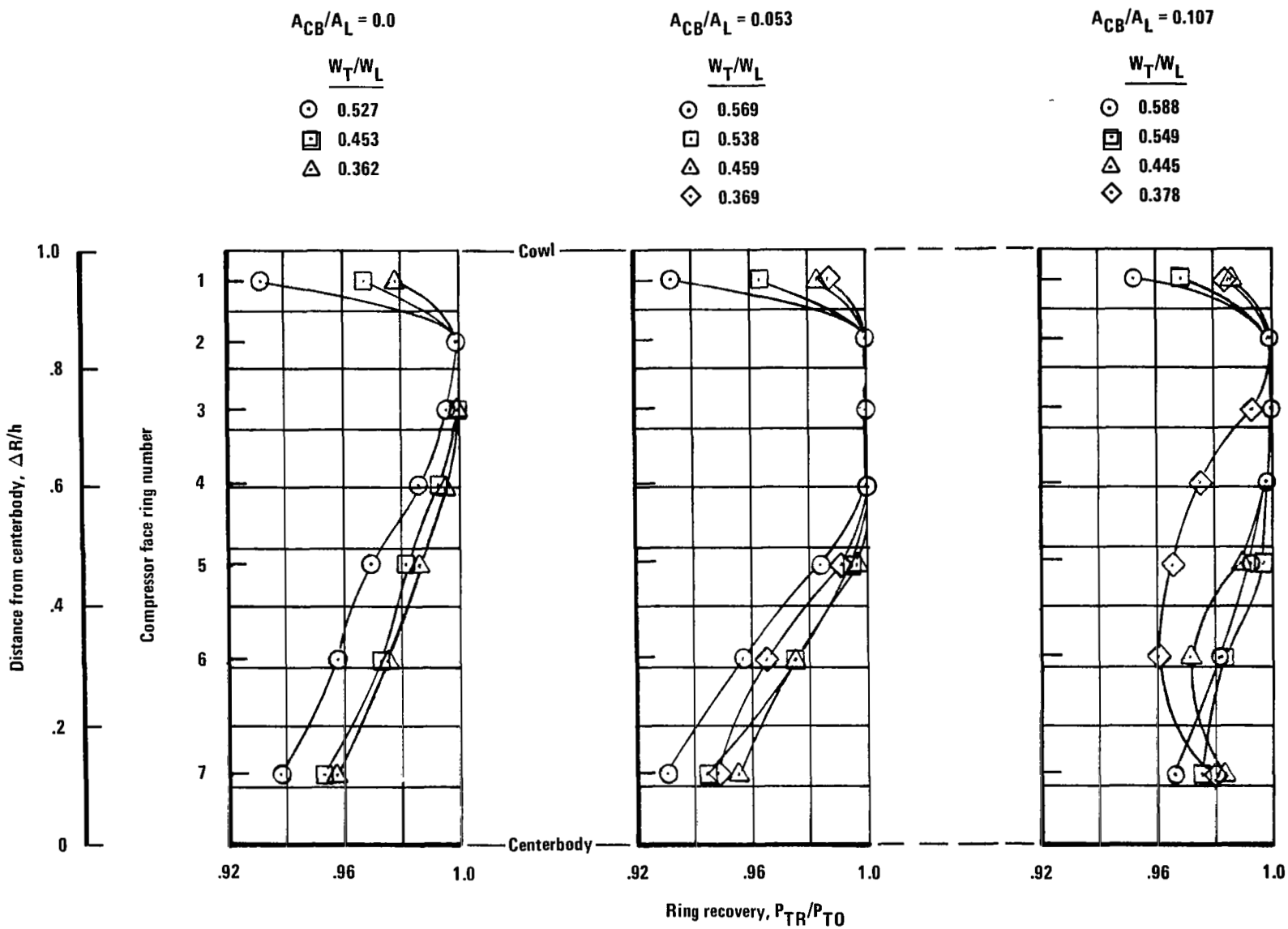

Figure 24.–Effect of Auxiliary Flow on Compressor-Face Ring Recovery, M_L = 0.9

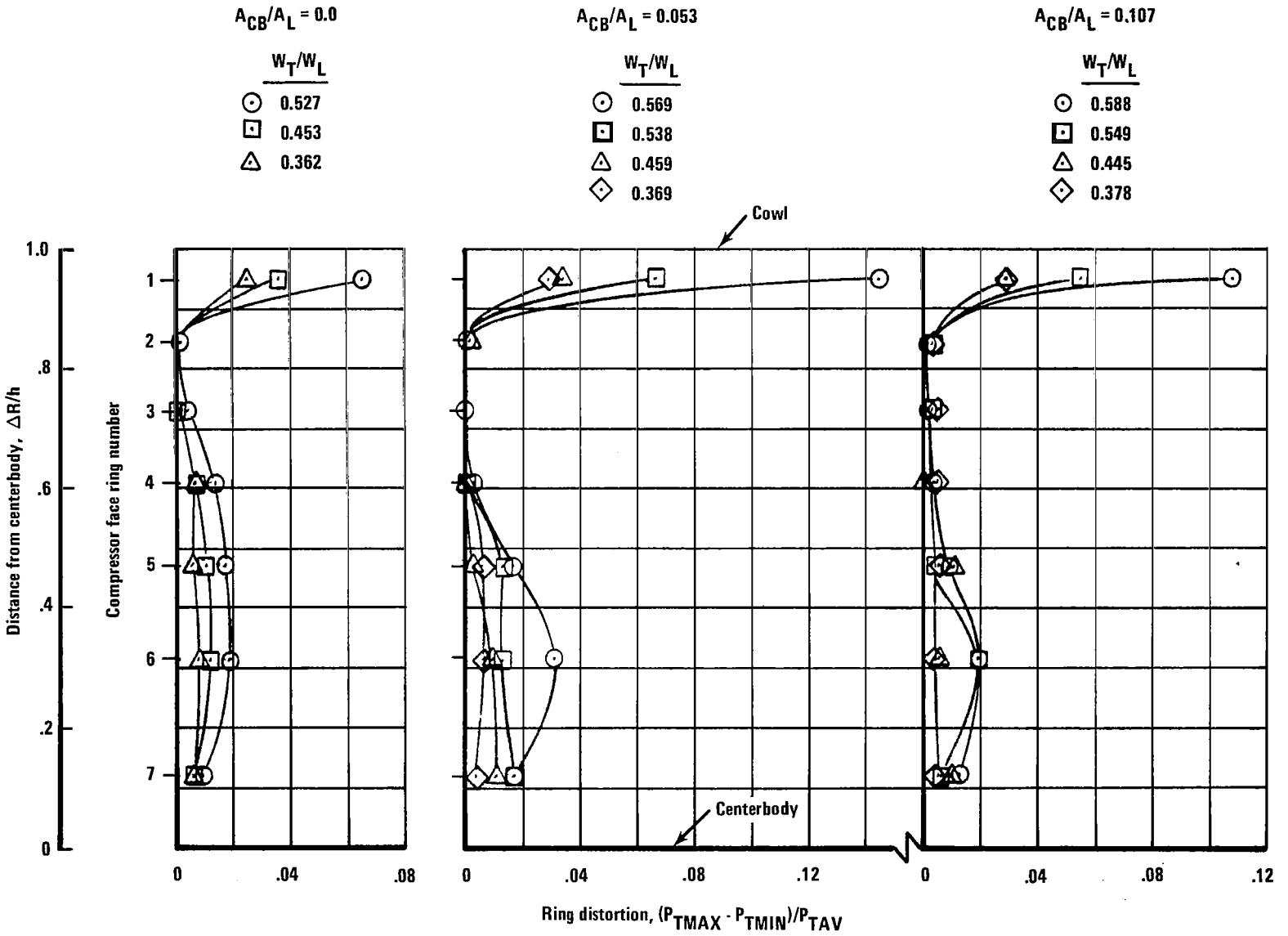

Figure 25.–Effect of Auxiliary Flow on Compressor-Face Ring Recovery, M_L = 0.9

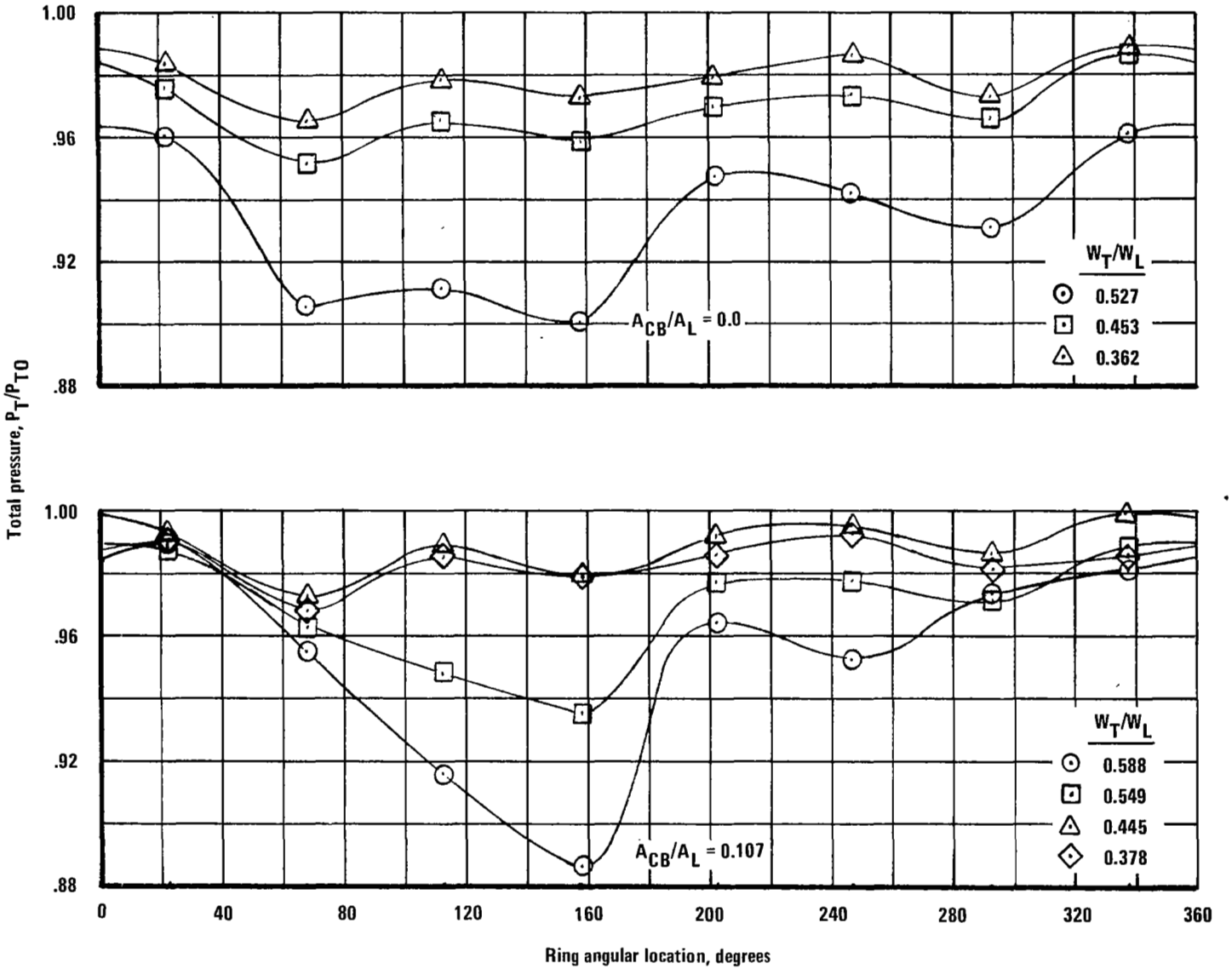

Figure 26.–Compressor-Face Ring Number One Total-Pressure Variation, $M_L = 0.9$

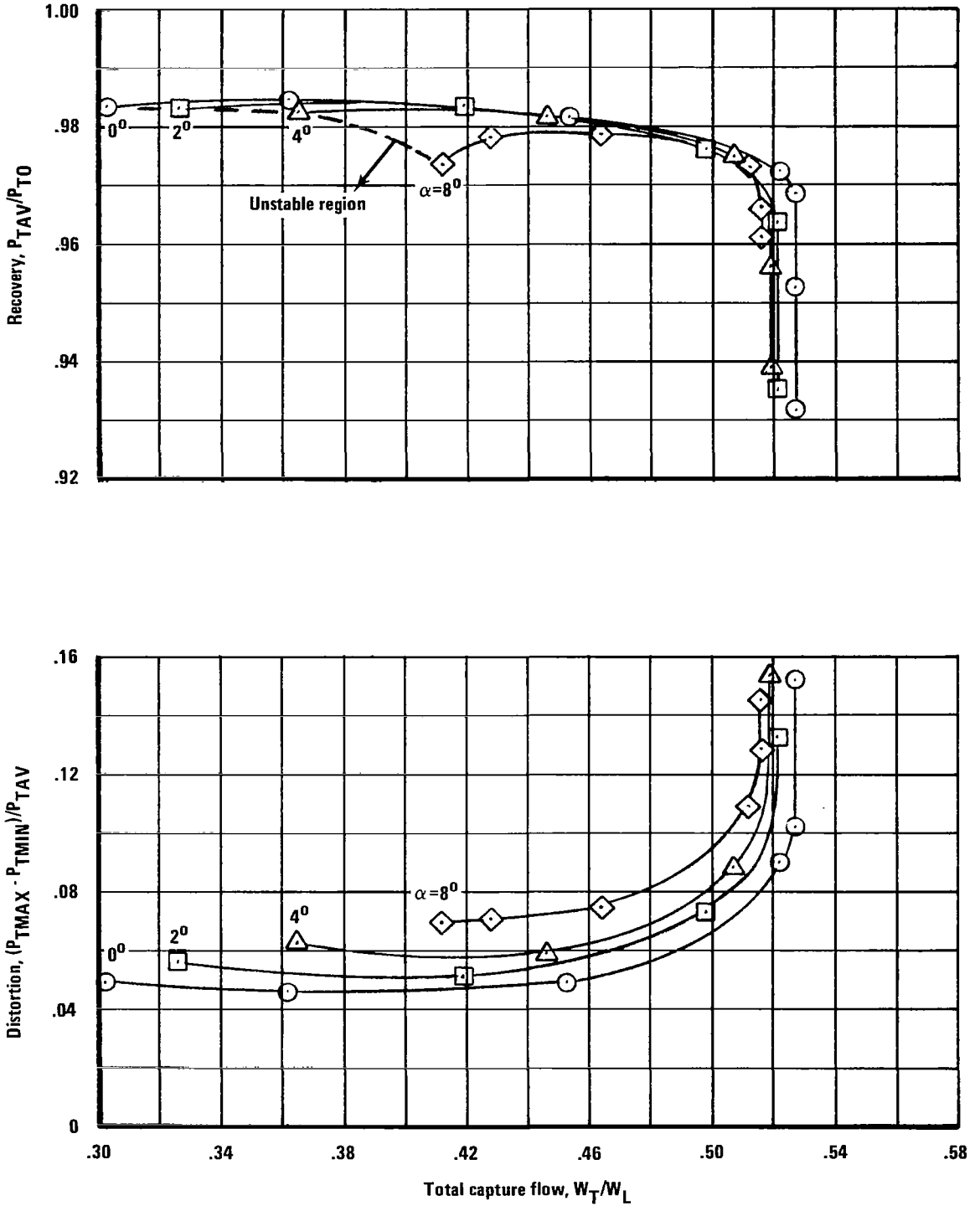

Figure 27.–Effect of Angle of Attack on Compressor-Face Performance, $M_L = 0.9$, $A_{CB}/A_L = 0$

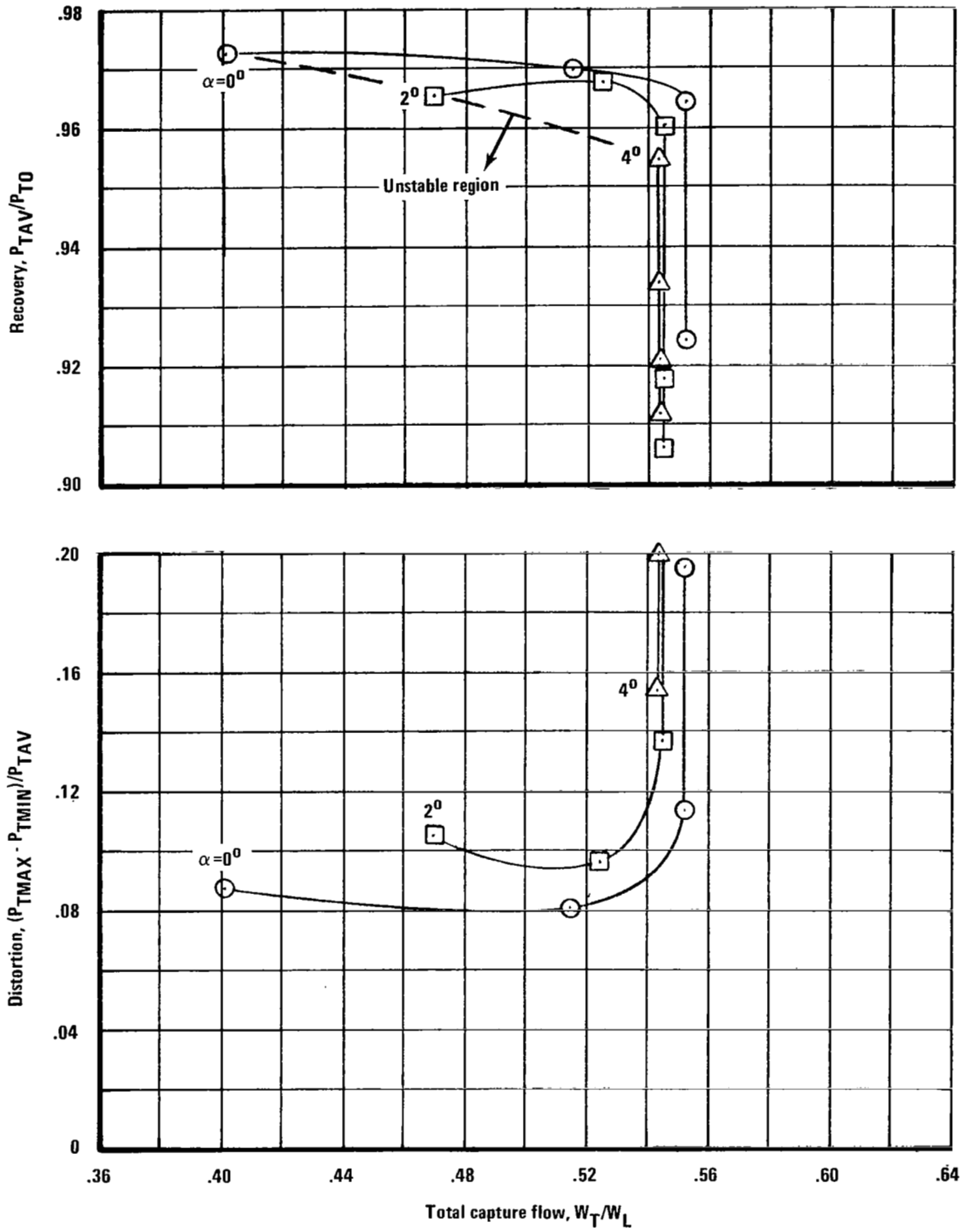

Figure 28.–Effect of Angle of Attack on Compressor-Face Performance, $M_L = 1.3$, $A_{CB}/A_L = 0$

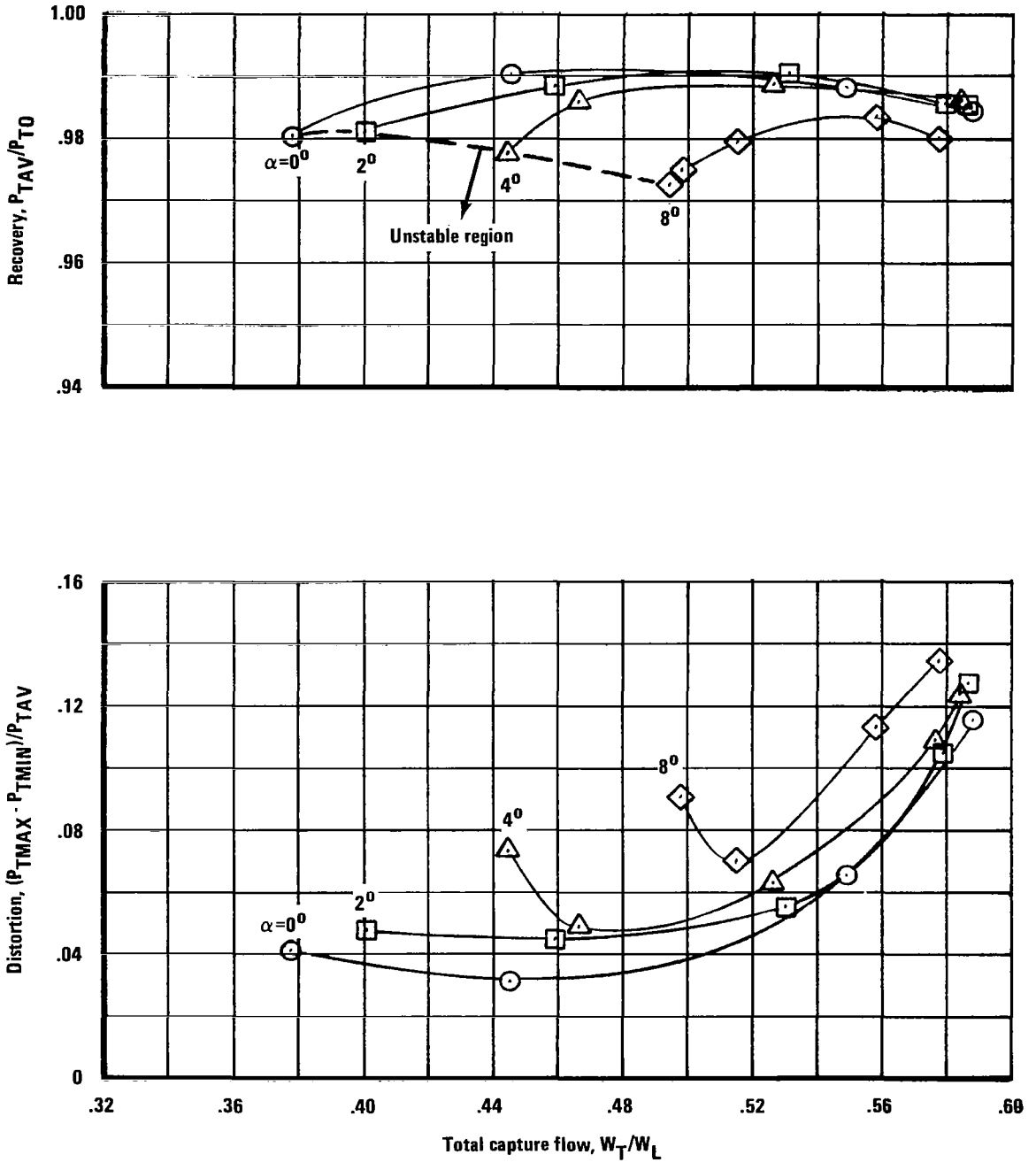

Figure 29.—Effect of Angle of Attack on Compressor-Face Performance, $M_L = 0.9$, $A_{CB}/A_L = 0.107$

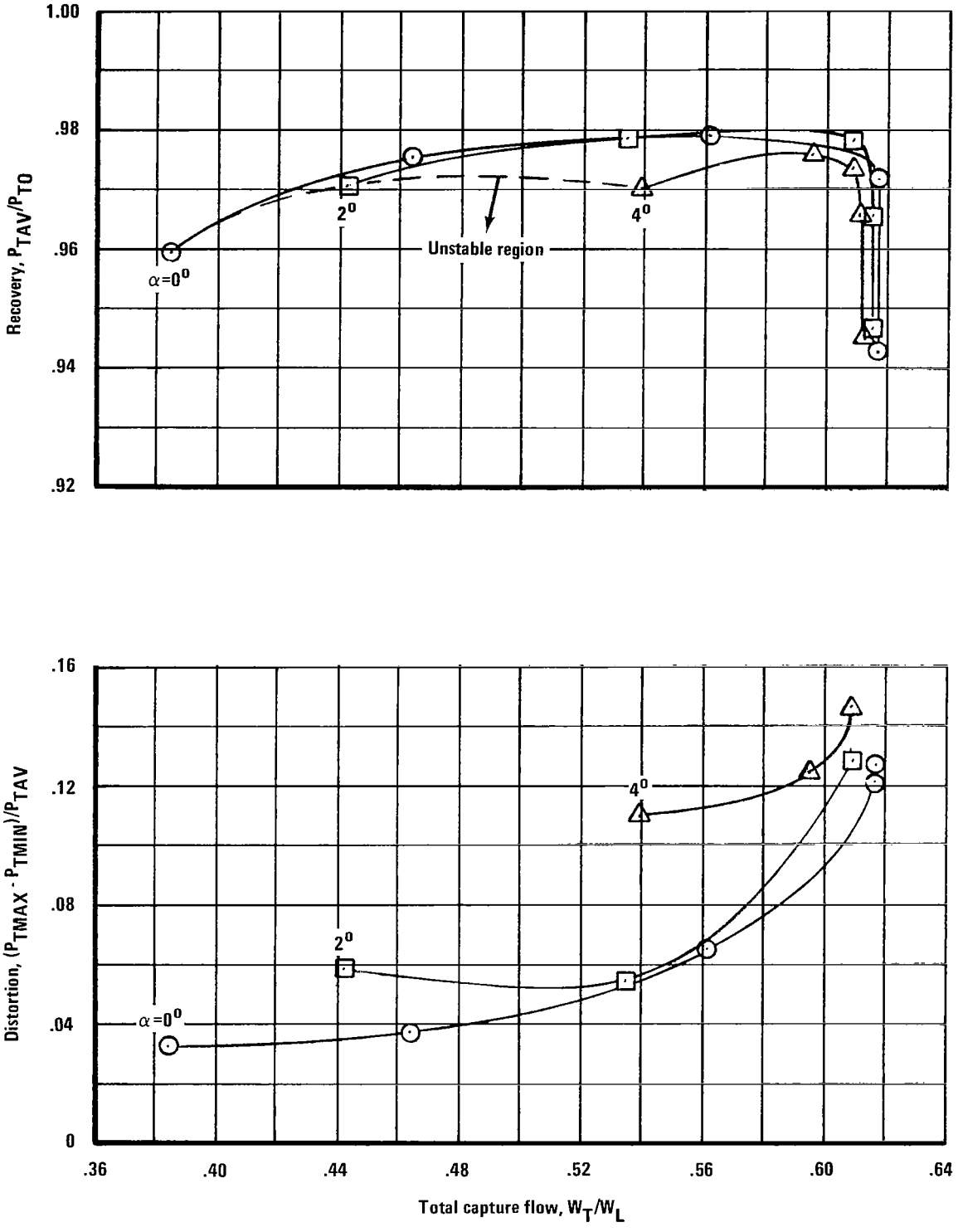

Figure 30.–Effect of Angle of Attack on Compressor-Face Performance, $M_L = 1.3$, $A_{CB}/A_L = 0.107$

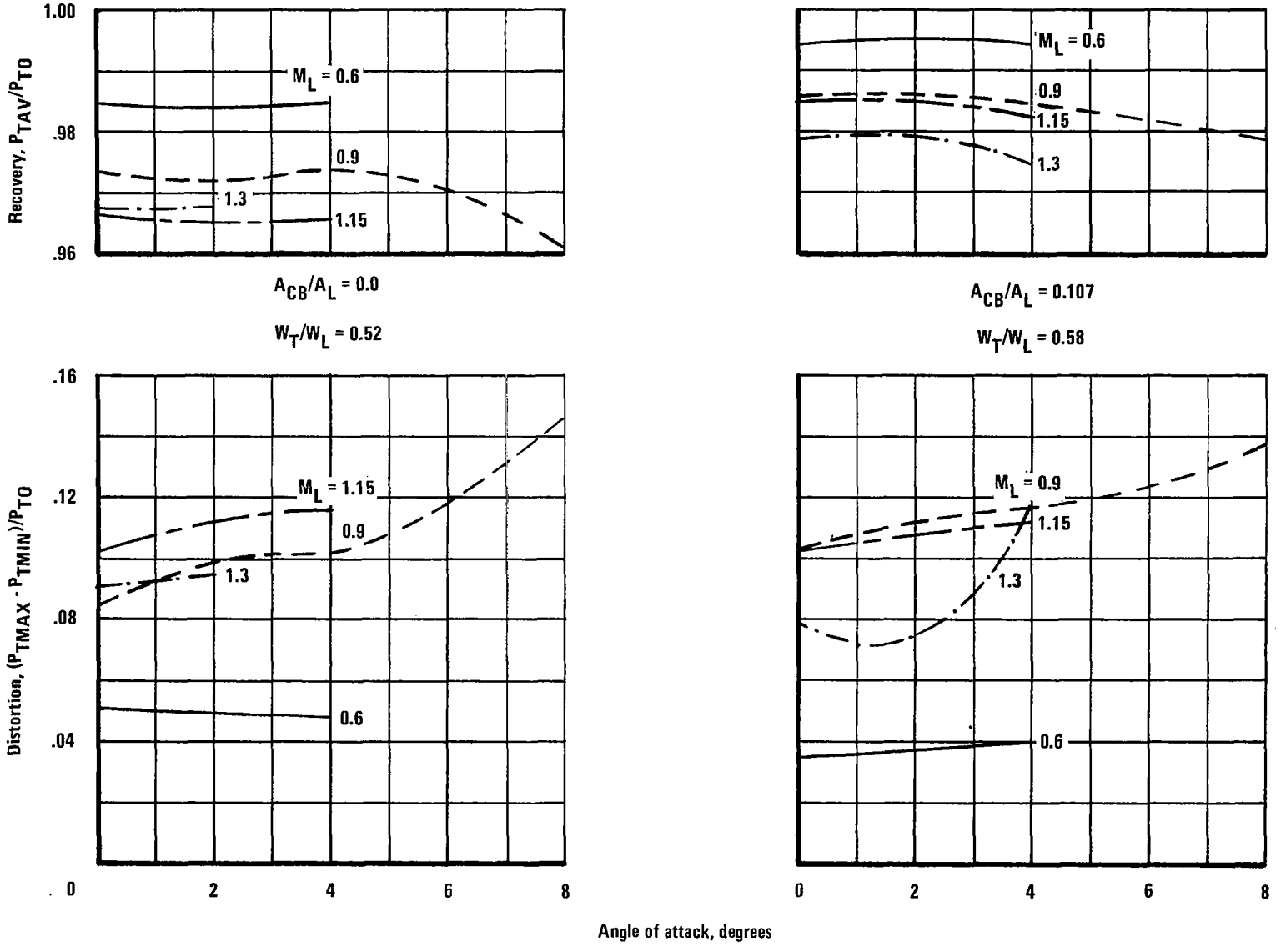

Figure 31.– Summary of Angle of-Attack Effects

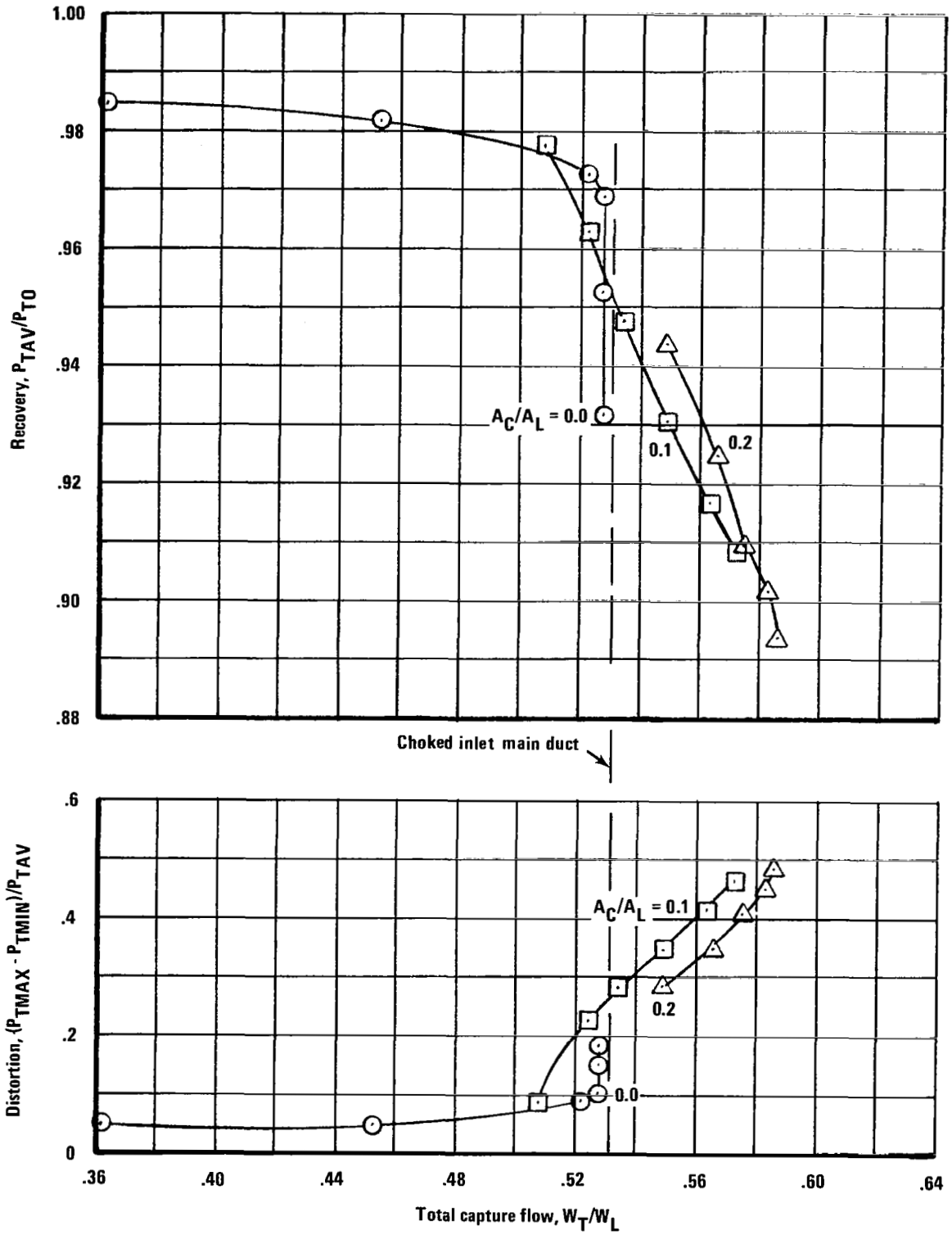

Figure 32.–Inlet Performance with Cowl Auxiliary Flow, $M_L = 0.9$

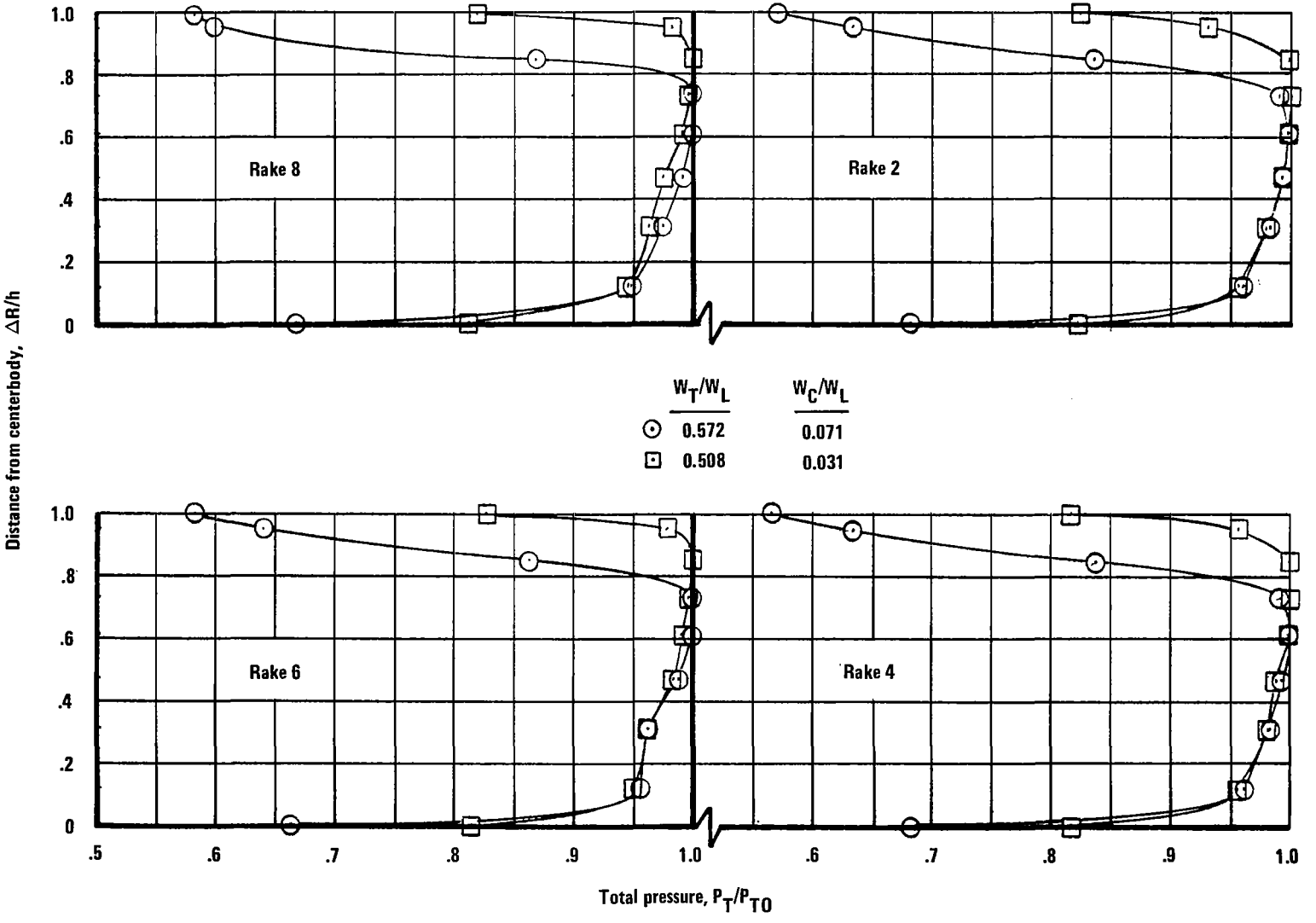

Figure 33.–Effect of Cowl Auxiliary Flow on Compressor-Face Rake Profiles, $M_L = 0.9$, $A_C/A_L = 0.1$

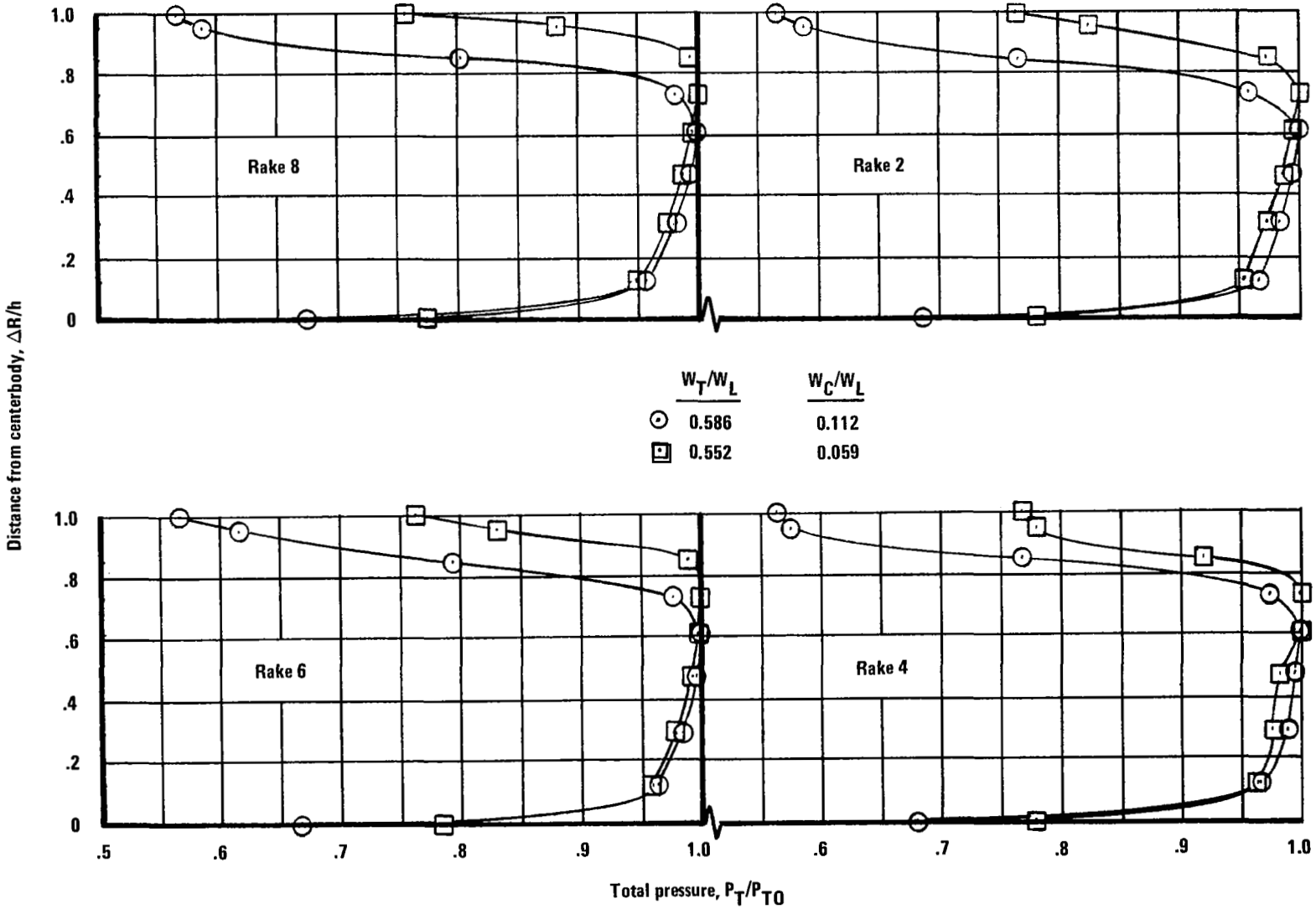

Figure 34.–Effect of Cowl Auxiliary Flow on Compressor-Face Rake Profiles, $M_L = 0.9$, $A_C/A_L = 0.2$

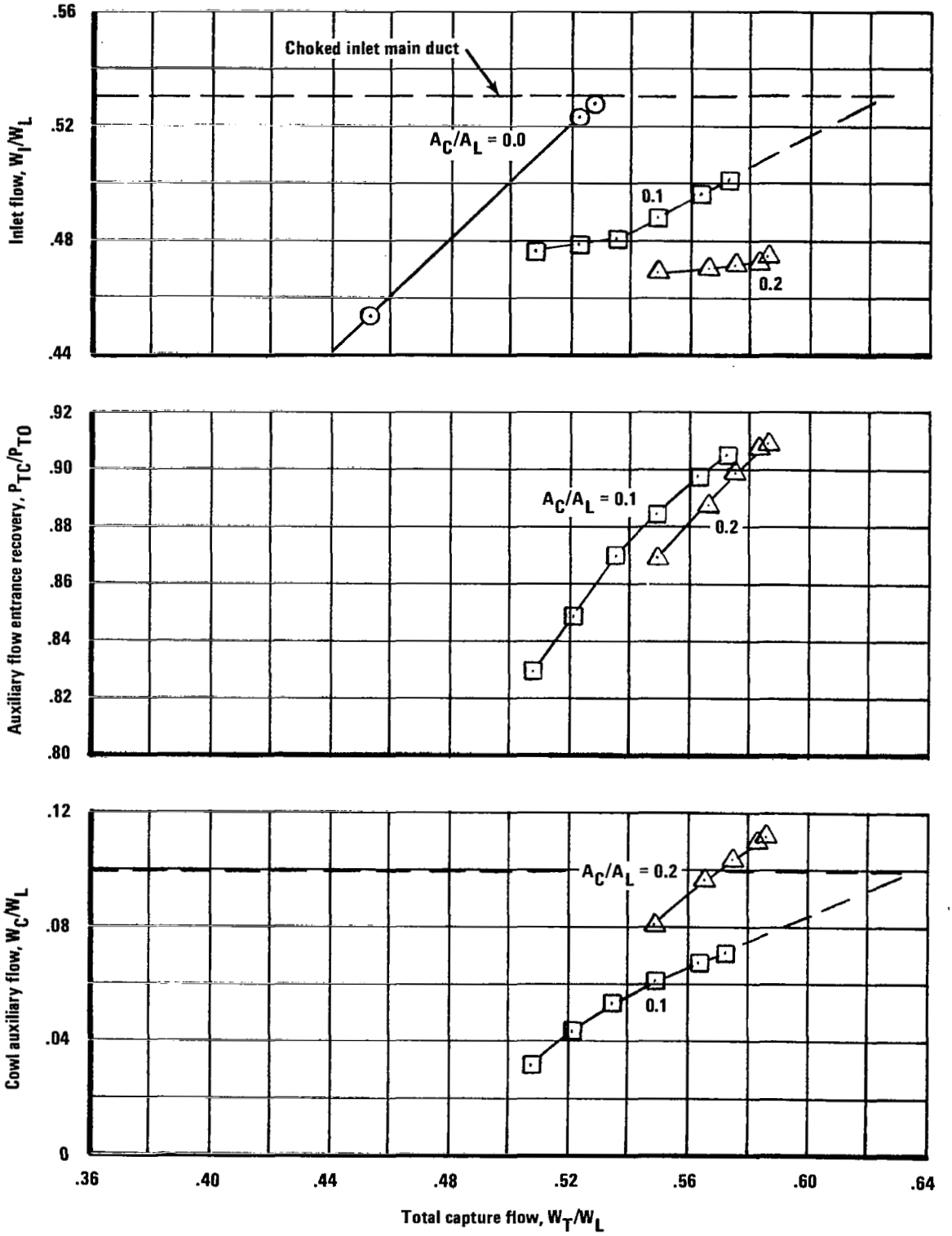

Figure 35.–Inlet/Cowl-Auxiliary-Duct Flow Characteristics, M_L = 0.9

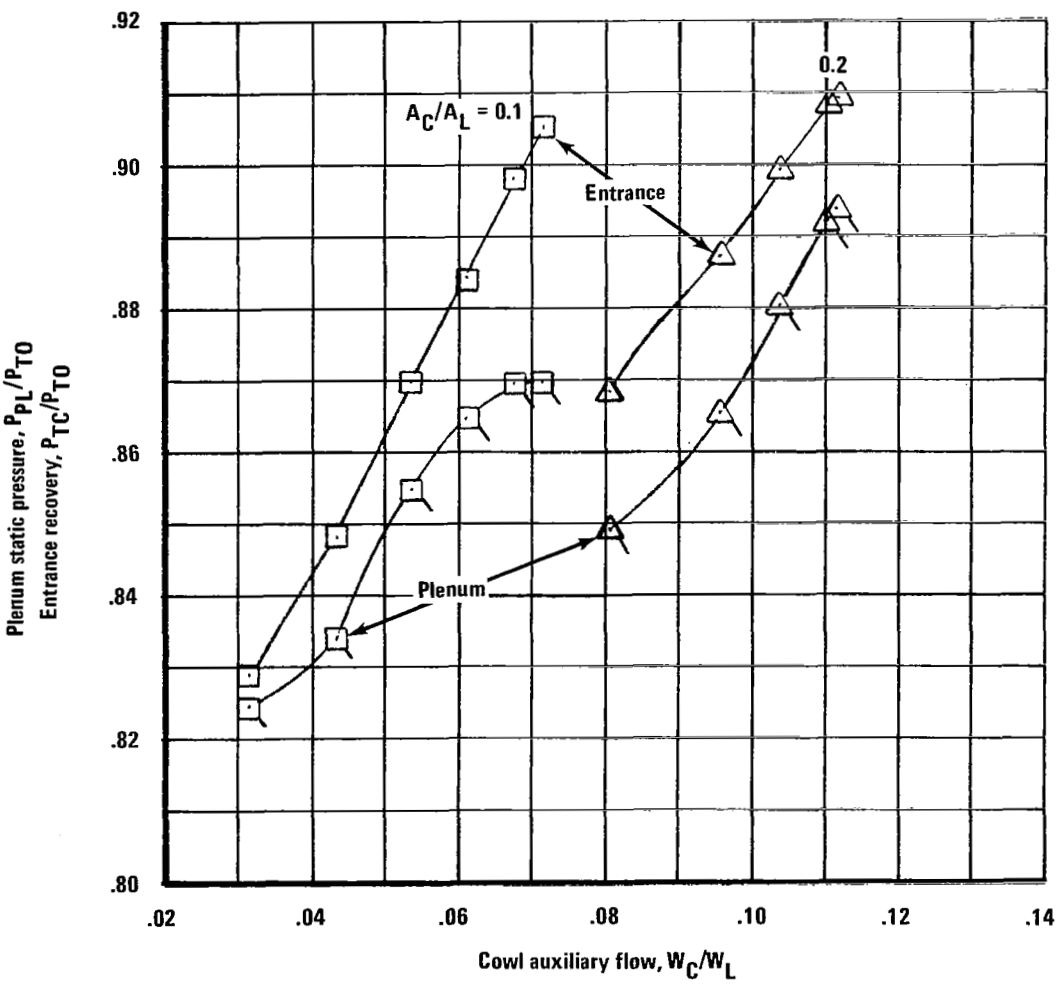

Figure 36.–Cowl Auxiliary Duct Performance Characteristics, M_L = 0.9

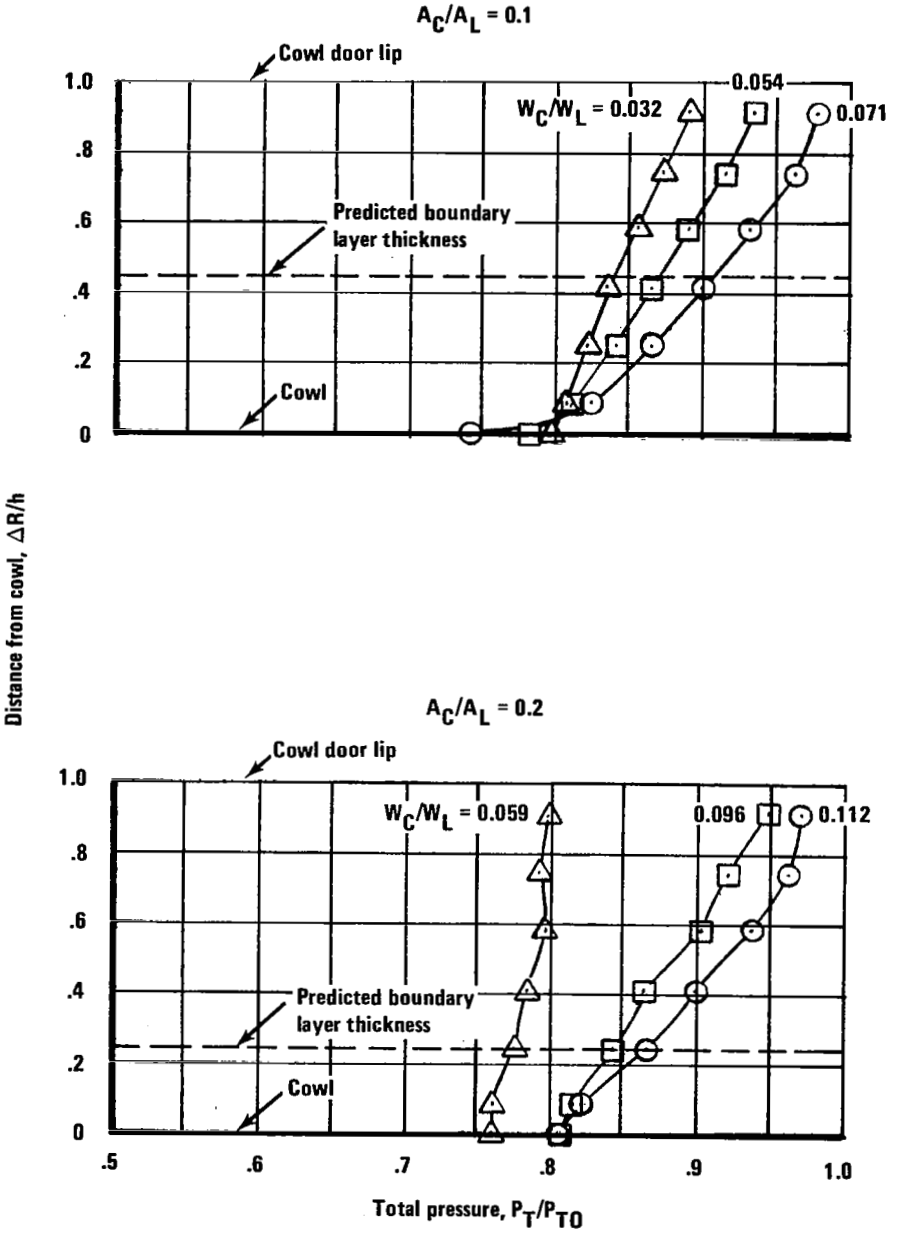

Figure 37.–Cowl Auxiliary Duct Entrance Total-Pressure Profiles, M_L = 0.9

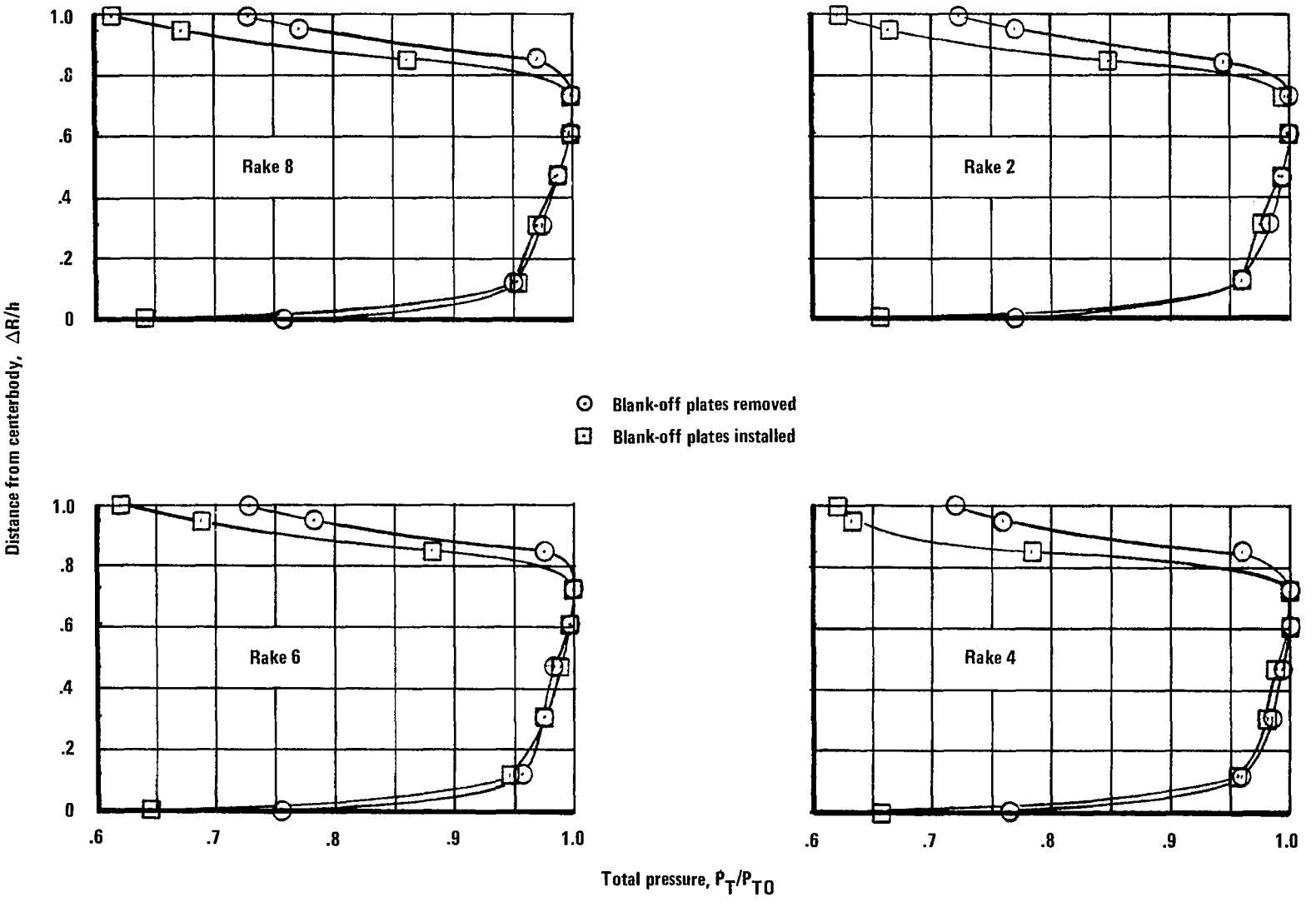

Figure 38.–Effect of Blank-Off Plates on Compressor-Face Total-Pressure Profiles, $M_L = 0.9$, $A_C/A_L = 0.1$, $W_C/W_L = 0.052$

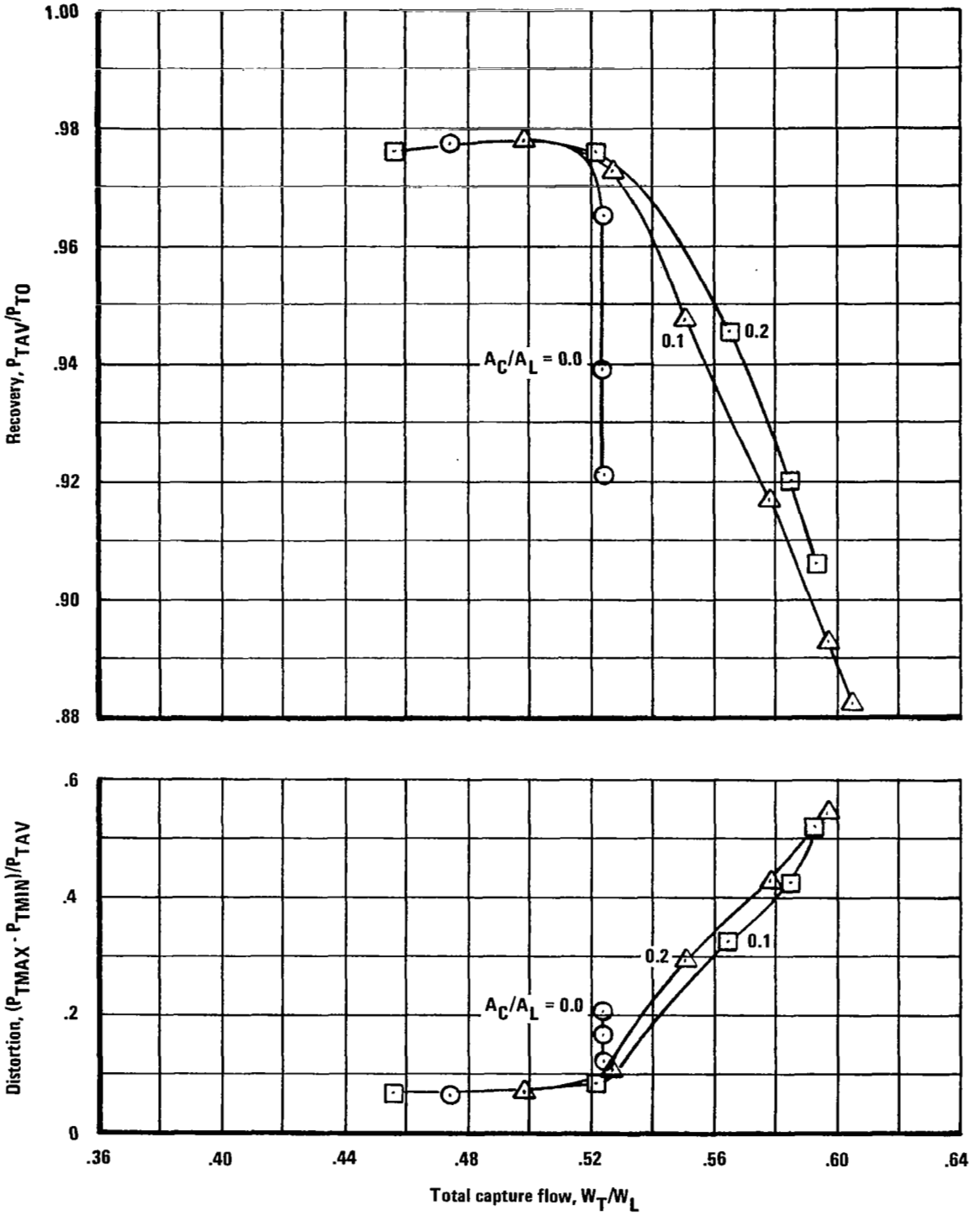

Figure 39.—Intake Performance with Cowl Auxiliary Flow, M_L = 1.15

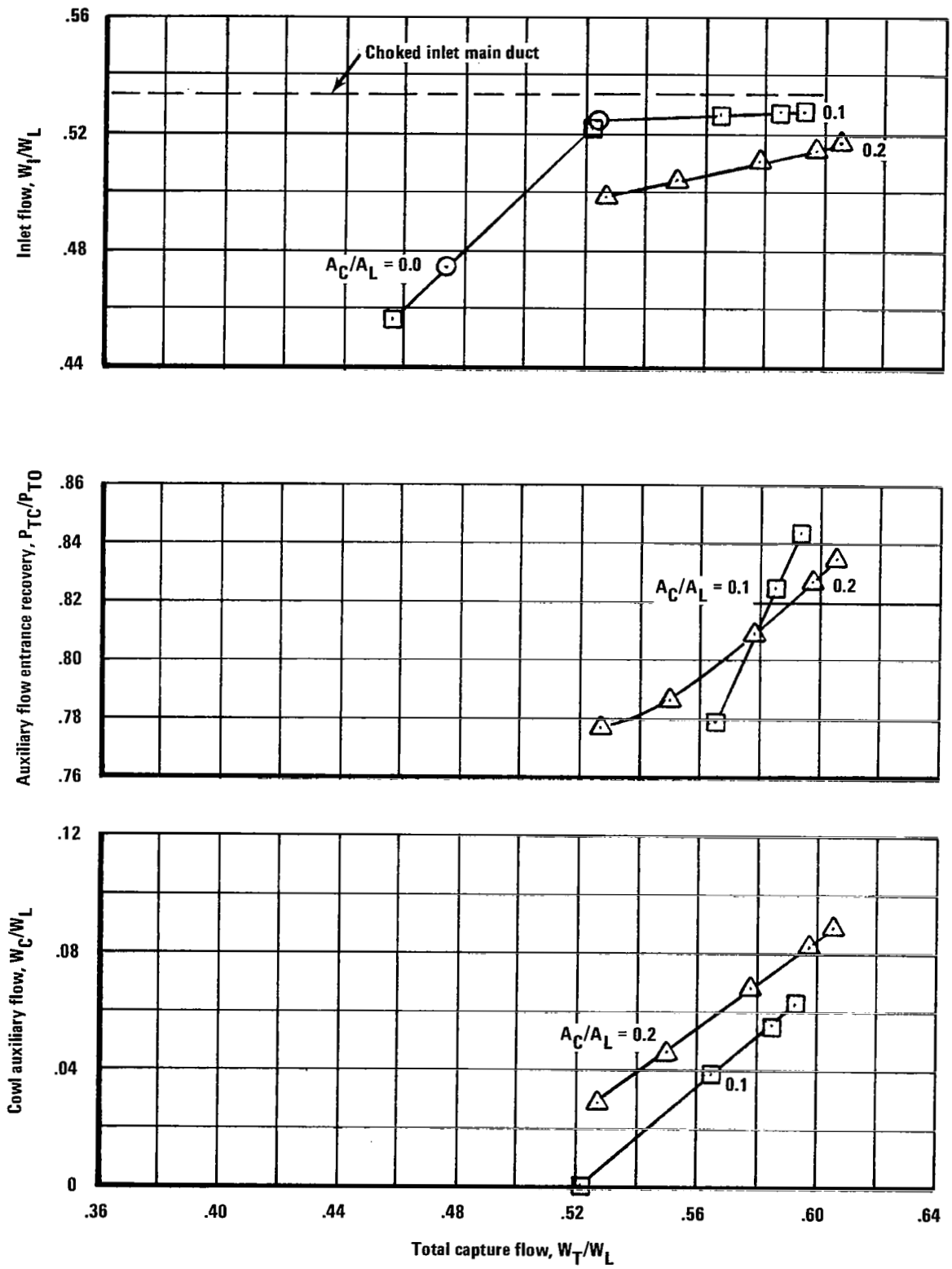

Figure 40.—Inlet/Cowl-Auxiliary-Duct Flow Characteristics, M_L = 1.15

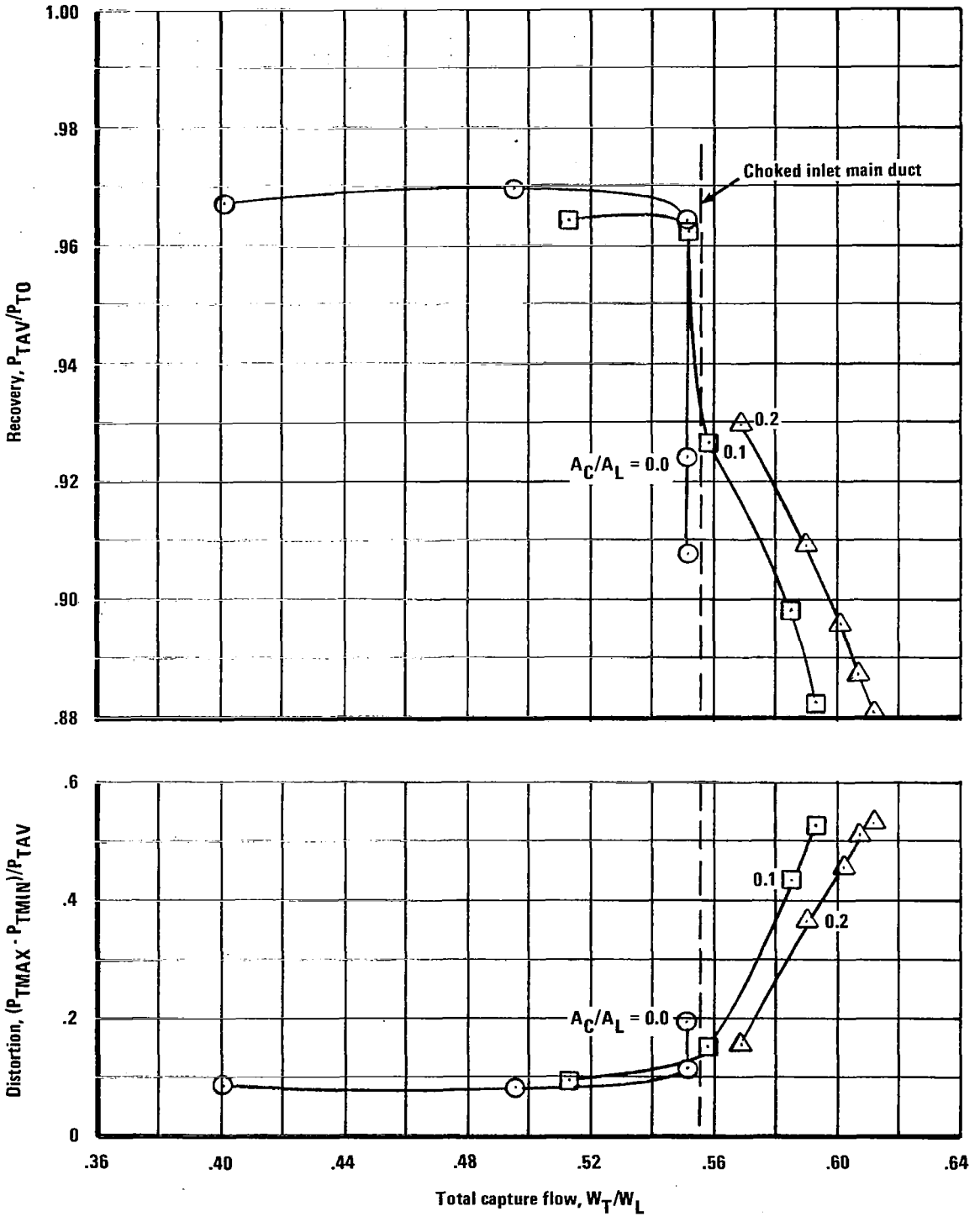

Figure 41.–Inlet Performance with Cowl Auxiliary Flow, M_L = 1.3

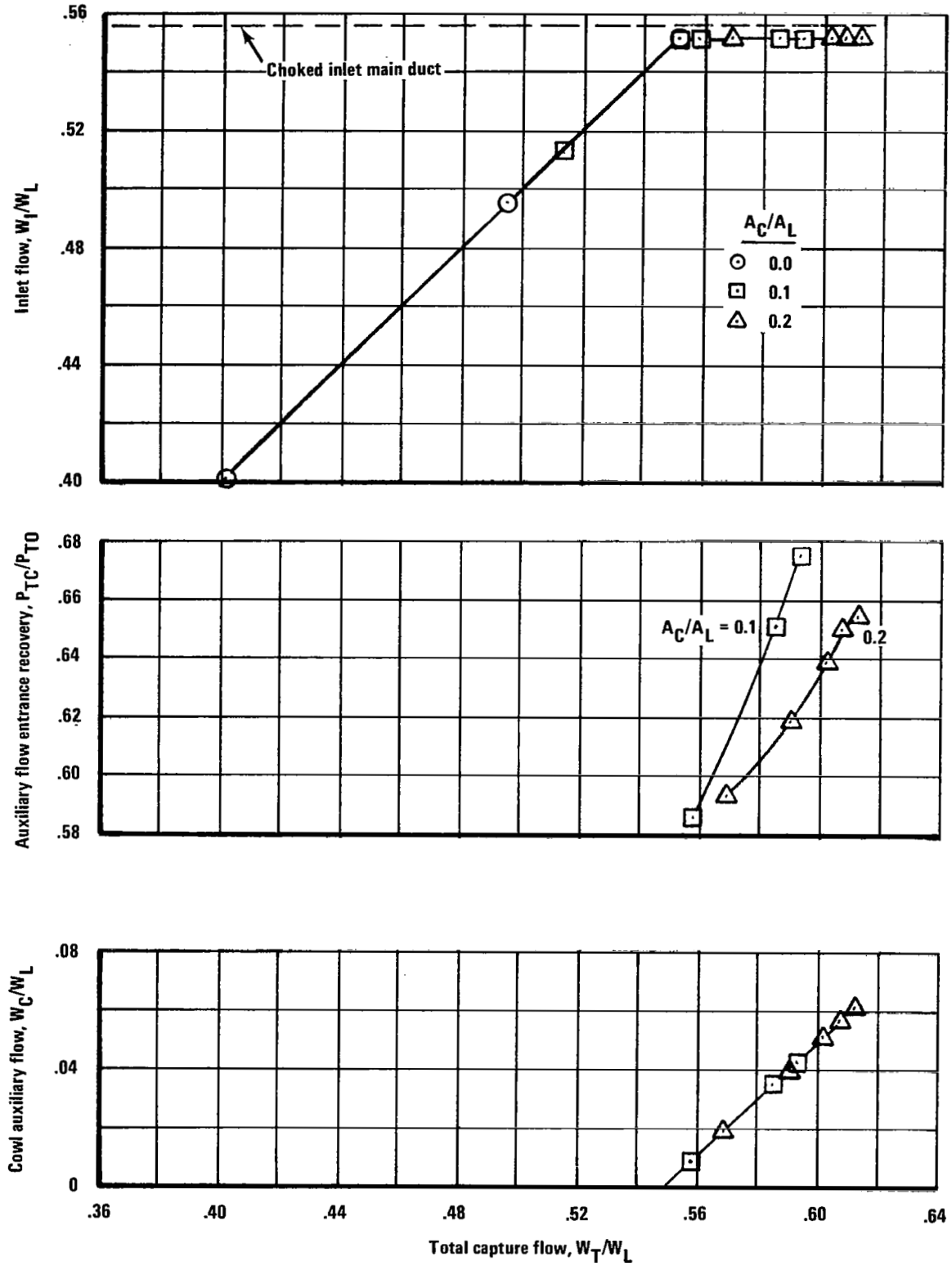

Figure 42.–Inlet/Cowl-Auxiliary-Duct Flow Characteristics, M_L = 1.3

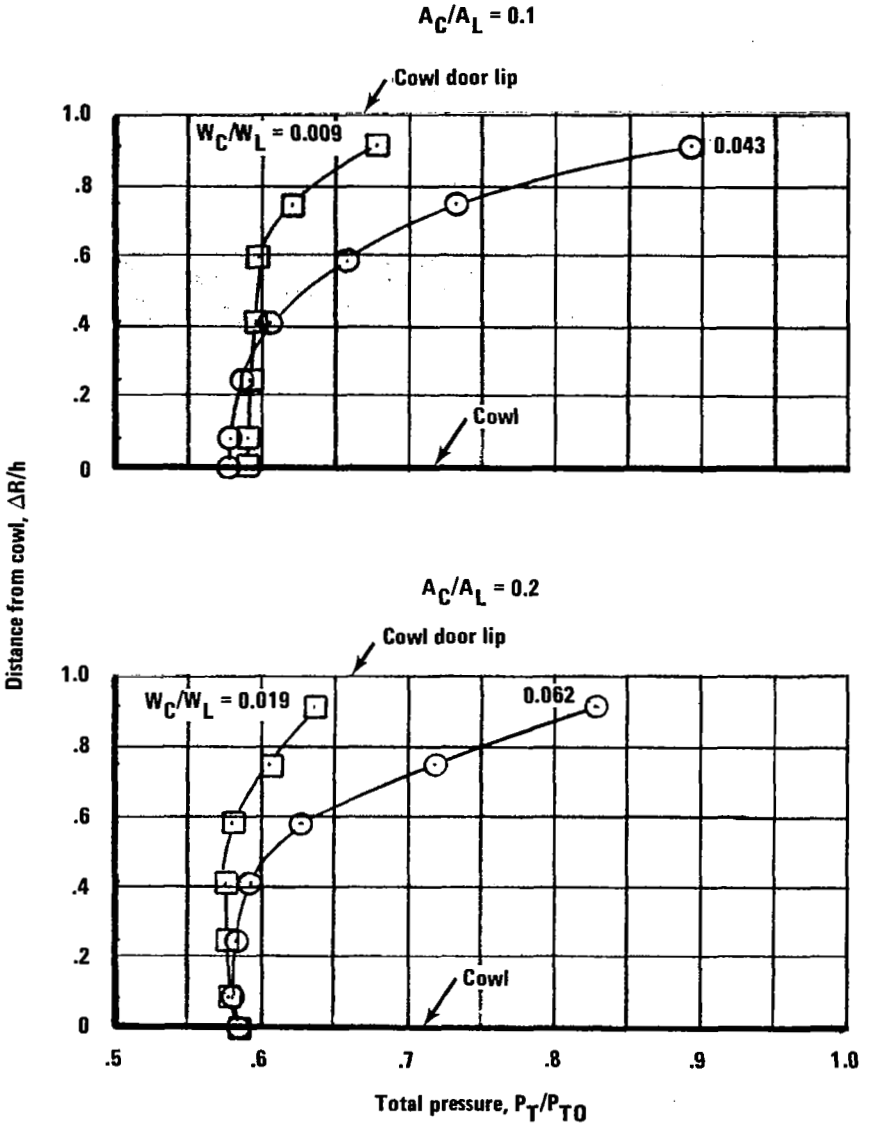

Figure 43.—Cowl Auxiliary Duct Entrance Total Pressure Profiles, M_L = 1.3

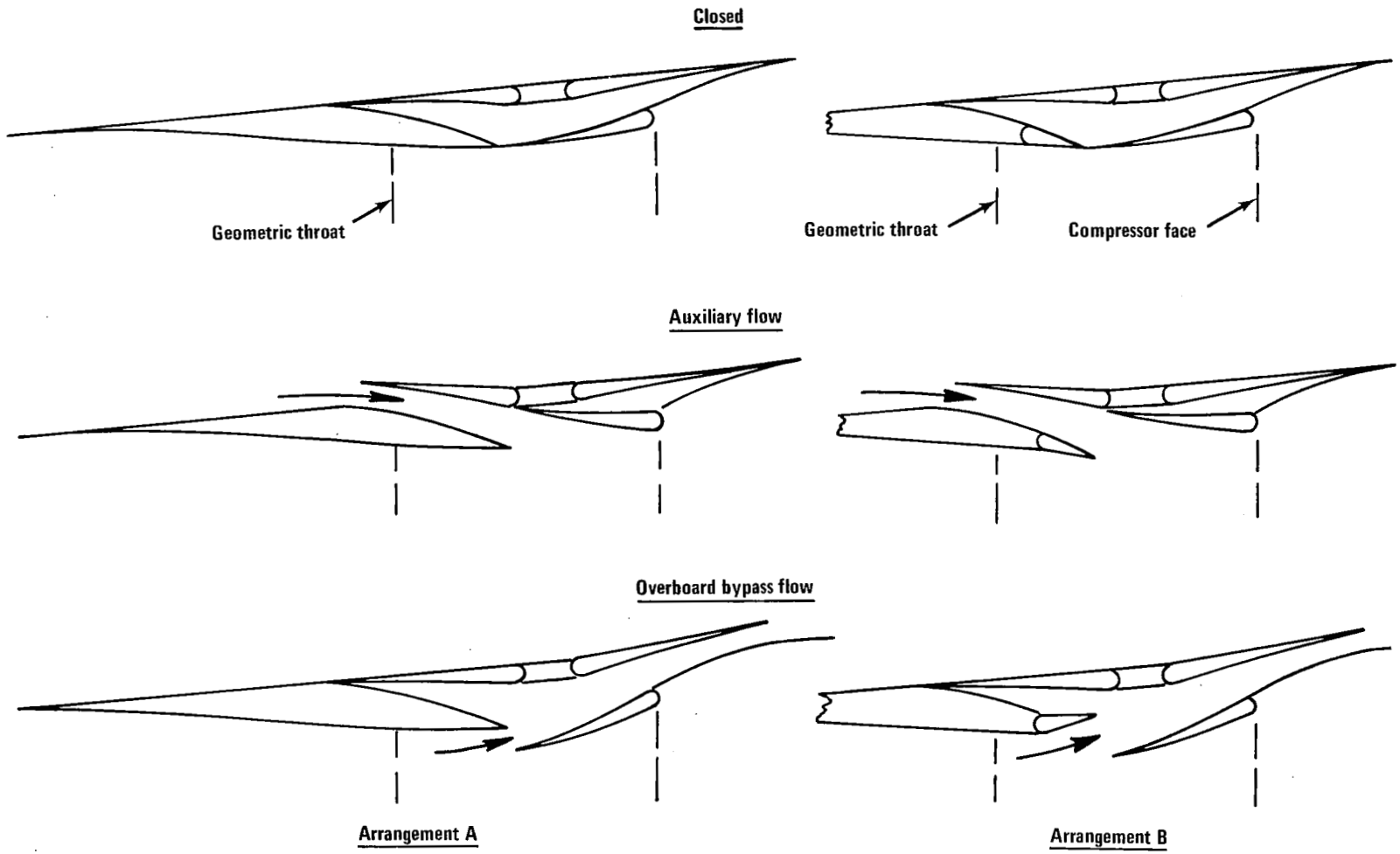

Figure 44.–Alternate Auxiliary Cowl Systems

Table I. – On-Design Contours
(centerbody fairing removed)

Station X/R_L	Radius, R/R_L	
	Centerbody	Cowl
1.360	0	
	9° Cone	
3.685	0.3637	1.0000
3.810	0.3880	1.0022
3.860	0.3959	1.0030
3.960	0.4119	1.0046
4.060	0.4283	1.0061
4.160	0.4452	1.0075
4.260	0.4632	1.0081
4.360	0.4814	1.0080
4.460	0.5005	1.0067
4.560	0.5202	1.0043
4.660	0.5403	1.0006
4.760	0.5614	0.9955
4.860	0.5830	0.9891
4.960	0.6050	0.9815
5.060	0.6265	0.9729
5.160	0.6461	0.9644
5.260	0.6625	0.9557
5.360	0.6759	0.9467
5.460	0.6865	0.9375

Station X/R_L	Radius, R/R_L	
	Centerbody	Cowl
5.560	0.6954	0.9275
5.610	0.6989	0.9219
5.660	0.7013	0.9166
5.710	0.7000	0.9119
5.760	0.6950	0.9080
5.810	0.6886	0.9050
5.860	0.6810	0.9020
5.960	0.6651	0.8960
6.060	0.6475	0.8900
6.160	0.6271	0.8850
6.260	0.6020	0.8825
6.360	0.5720	0.8852
6.460	0.5350	0.8920
6.535	0.5040	0.8980
6.535	0.3125	0.8980
6.560	0.3145	0.9000
6.660	0.3226	0.9084
6.760	0.3307	0.9170
6.810	0.3348	0.9225
6.860	0.3389	0.9300
6.910	0.3429	0.9370
6.960	0.3470	0.9390

Table II. – Centerbody Fairing and Support Strut Contours

Centerbody Fairing

Station X/R_L	R/R_L
6.360	0.3125
6.410	0.3465
6.460	0.3786
6.510	0.4062
6.560	0.4264
6.610	0.4389
6.660	0.4388
6.710	0.4270
6.760	0.4058
6.810	0.3843
6.860	0.3660
6.910	0.3555
6.960	0.3470

Support Strut

Station X/R_L	Thickness t/R_L
6.235	0.000
6.360	0.076
6.460	0.138
6.560	0.186
6.660	0.206
6.760	0.190
6.860	0.136
6.960	0.064